Gold solubility and speciation in hydrothermal solutions: experimental study of the stability of hydrosulphide complex of gold (AuHS°) at 350 to 450°C and 500 bars

Francois Gibert, Marie-Lola Pascal, Michel Pichavant

Pergamon

Gold solubility and speciation in hydrothermal solutions: Experimental study of the stability of hydrosulphide complex of gold (AuHS°) at 350 to 450°C and 500 bars

F. Gibert,[1,2,]* M.-L. Pascal,[1] and M. Pichavant[1]

[1]CRSCM-CNRS, 1a rue de la Ferollerie, 45071 Orléans, France
[2]Université Blaise Pascal, UMR 6524 du CNRS, 5 rue Kessler, 63038 Clermont-Ferrand, France

Abstract—The solubility of gold was measured in aqueous KCl (0.5 m) solutions under oxygen, sulfur, and slightly acidic pH buffered conditions between 350 and 450°C at a constant pressure of 500 bars. Two buffer assemblages were used to constrain fO_2, fS_2, and consequently fH_2 and aH_2S: respectively, pyrite-pyrrhotite-magnetite (Py-Po-Mt) and pyrite-magnetite-hematite (Py-Mt-Hm). The measured solubility of gold at equilibrium with Py-Po-Mt and Qtz-KF-Mus is 52 ± 8 ppb at 350°C, 134 ± 17 ppb at 400°C and 496 ± 37 ppb at 450°C. With Py-Mt-Hm and Qtz-KF-Mus the solubility of gold is increased to 198 ± 9 ppb at 400°C and 692 ± 10 ppb at 450°C. These results are consistent with the aqueous complex AuHS° being the dominant gold-bearing species. The equilibrium constants (log K_{R10}) for the reaction:

$$Au_{(s)} + H_2S_{(aq)} = AuHS^0 + \tfrac{1}{2} H_{2(g)} \qquad \text{R10}$$

have been determined at 350, 400, and 450°C and are, respectively, −5.20 ± 0.25, −5.30 ± 0.15, and −5.40 ± 0.15. These values are similar to those suggested by Zotov (written pers. commun.) and those obtained by recalculating the experimental data of Hayashi and Ohmoto (1991). They are significantly higher than those derived by Benning and Seward (1996) and the possible causes of the discrepancies are discussed.

The equilibrium constant for AuHS° shows that this species plays an important role in the deposition of gold in natural environments. Cooling, H_2S loss, pH change, and oxidation seem to be effective mechanisms for gold precipitation, depending on the local ore forming conditions. *Copyright © 1998 Elsevier Science Ltd*

1. INTRODUCTION

Field and mineralogical studies of hydrothermal gold deposits demonstrate the large range of physicochemical conditions of gold deposition. This suggests that different aqueous species can transport gold depending on temperature, pH, redox state, and ligand concentrations. Therefore, knowledge of the solubility of gold in hydrothermal fluids is critical in interpreting the transport and deposition of gold in ore-forming processes. The most important ligands in hydrothermal gold-bearing solutions are chloride and reduced sulphur. Both are known to form complexes with Au(I).

Several experimental studies have investigated the solubility and formation of complexes of gold in chloride solutions (Nikolaeva et al.,1972; Henley, 1973; Rytuba and Dickson, 1974; Wood et al., 1987). A more general study of the solubility of gold in aqueous chloride solutions (Zotov and Baranova, 1989) has provided thermodynamic data for the $AuCl_2^-$ species at temperatures from 350°C to 500°C and pressures from 500 to 1500 bars.

Previously, Seward (1973) has determined the stoichiometry and the stability constant of gold-sulphide complexes in aqueous sulphide solutions in the presence of pyrite and pyrrhotite. It was shown that the dominant gold-bearing species is either $Au(HS)_2^-$ in neutral to slightly alkaline solutions or $Au_2(HS)_2S^-$ in strongly alkaline solutions, at temperatures from 175°C to 250°C and a pressure of 1 kbar. In addition, it was suggested that a pH independent species, AuHS°, is present in the acidic region. Shenberger and Barnes (1989) have also measured gold solubilities in chlorine-free sulphide solutions. For temperatures from 150°C to 300°C under vapour-saturated (Psat) and high fO_2 conditions, they found that $Au(HS)_2^-$ was the dominant gold complex and also suspected the presence of a neutral complex (AuHS°) in their low pH runs. A neutral complex has been also identified at low temperatures by Renders and Seward (1989) who measured the solubility of $AuS_2(s)$ at 25°C and for pH between 2 to 12. They determined that the dominant gold species was AuHS° at pH 3 to 3.5, $Au(HS)_2^-$ at pH 4 to 10 and $Au_2S_2^{2-}$ at pH above 11. These findings contrast with Seward (1984), who suggested that $HAu(HS)_2^\circ$ might be the dominant species in low pH solutions. Hayashi and Ohmoto (1991) have measured gold solubility from 250°C to 350°C at Psat in chloride and sulphide-bearing aqueous solutions buffered by a sulphur hydrolysis reaction and sulphate-sulphide equilibrium. Their data indicate the existence of a neutral, pH independent, gold species with an $HAu(HS)_2^\circ$ stoichiometry. Recently, two other studies (Benning and Seward, 1993, 1995, 1996; Gibert et al., 1993) have inferred an AuHS° stoichiometry for the neutral species.

In this paper, we present the results of gold solubility measurements between 350°C and 450°C at 500 bars in aqueous chloride solutions with sulfur and hydrogen fugacities buffered by assemblages of iron-sulphides and iron-oxides (pyrite, pyrrhotite, magnetite, and hematite). These mineral assemblages are commonly found in association with gold in many hydrothermal deposits. The results of this study confirm that AuHS° plays an important role in the deposition of gold in natural

---

*Author to whom correspondence should be addressed (gibert@opgc.univ-bpclermont.fr).

environments and promote a better understanding of the transport and deposition of gold in natural hydrothermal systems.

2. EXPERIMENTAL METHODS

The experiments were designed to simulate the condition of gold transport in natural hydrothermal systems as closely as possible, while allowing for precise control of the experimental parameters (T, pH, $f\mathrm{H}_2$, $f\mathrm{S}_2$).

2.1. Choice of Experimental Conditions

Our strategy is based on the modelling of the solubility and the speciation of gold in an $\mathrm{H}_2\mathrm{O}$-KCl solution in chemical equilibrium with $f\mathrm{O}_2$-$f\mathrm{S}_2$ buffer pyrite-pyrrhotite-magnetite (Py-Po-Mt) and pH buffer quartz-K-feldspar-muscovite (Qtz-KF-Mus) at 350°C and vapor-saturated pressure (Gibert and Pascal, 1992). At 350°C and Psat, results of the modelling show that $\mathrm{Au(HS)}_2^-$ is the dominant gold-bearing species in alkaline solutions and that AuCl_2^- is significant only in solutions with high $\Sigma\mathrm{Cl}$ or at low pH conditions. A neutral species ($\mathrm{AuHS}°$ or $\mathrm{HAu(HS)}_2°$) is likely to be the dominant gold carrier in solutions with neutral pH. With increasing temperature, the region of dominant $\mathrm{Au(HS)}_2^-$ is shifted to more alkaline conditions. Thus, at high temperatures (T > 350°C) and in equilibrium with sulphide minerals (Py, Po), $\mathrm{Au(HS)}_2^-$ plays relatively minor role in gold transport in the pH range 5–6.5. Within these premises, we have measured gold concentrations in a 0.5 m KCl aqueous solution in equilibrium with $f\mathrm{O}_2$-$f\mathrm{S}_2$ and pH quartz-K-feldspar-muscovite (Qtz-KF-Mus) buffers between 350°C and 450°C at a constant pressure of 500 bars. For a precise determination of the stoichiometry of the gold species, the use of two redox buffers is necessary (Gibert et al., 1993). In our experiments either a pyrite-pyrrhotite-magnetite (Py-Po-Mt buffer) or a pyrite-magnetite-hematite (Py-Mt-Hm buffer) assemblage was used to buffer $f\mathrm{O}_2$, $f\mathrm{S}_2$, and consequently $f\mathrm{H}_2$ and $a\mathrm{H}_2\mathrm{S}$.

2.2. Apparatus

Experiments were performed using a rocking flexible-cell hydrothermal apparatus (Seyfried et al., 1987). Reactants (i.e, gold tube, solid buffers, and aqueous solution) were loaded into a deforming titanium reaction cell (50–160 mL, wall thickness 1/40″) with a Ti closure piece which was inserted into a 316SS autoclave. A Ti sampling tube extends from the closure piece of the cell to the external Ti sampling valve. The autoclave was placed into a rocking furnace and then filled with water which was used as the pressure medium. A small amount of SrCl_2 was added to the water pressure medium as a leak tracer. Initially, the vessel was pressurized to 20–30 bars to collapse the Ti cell. During this step, the Ti sampling valve was opened and the first drops of solution ($\approx$1 mL) were collected. This first sample was analysed by flame absorption spectrometry for Sr to detect any contamination of the experimental solution from the water pressure medium. Throughout the experiment temperature was controlled within $\pm$ 2°C and pressure was maintained within $\pm$20 bars. Before each experiment, all Ti pieces (cell, closure piece, filter, and exit tube) were first cleaned with a diluted HCl solution (0.1 N), then treated in concentrated nitric acid before being heated in air at 400°C to form a superficial chemically inert titanium oxide layer.

2.3. Starting Materials

Pyrite and pyrrhotite were synthetic phases prepared from a mixture of sulphur and iron sponge powders (both Prolabo Co., reagent pure) heated to 700°C for 6 days in vacuum-sealed silica tubes and then equilibrated during 24 h at the temperature of experiment (350–450°C). Magnetite, hematite and K-feldspar were prepared by hydrothermal synthesis (600°C, 2kbar). Mixtures of iron and hematite powders were used for the iron oxides; K-feldspar was synthesised from a gel. A synthetic commercial quartz (SICN Co.) and a natural muscovite from a pegmatite were also used. The buffer mineral assemblage was studied with X-ray diffraction, microprobe analysis, and SEM before and after each experiment. Figure 1 shows an example of the mineral assemblage after a run. Materials phases show subidio-
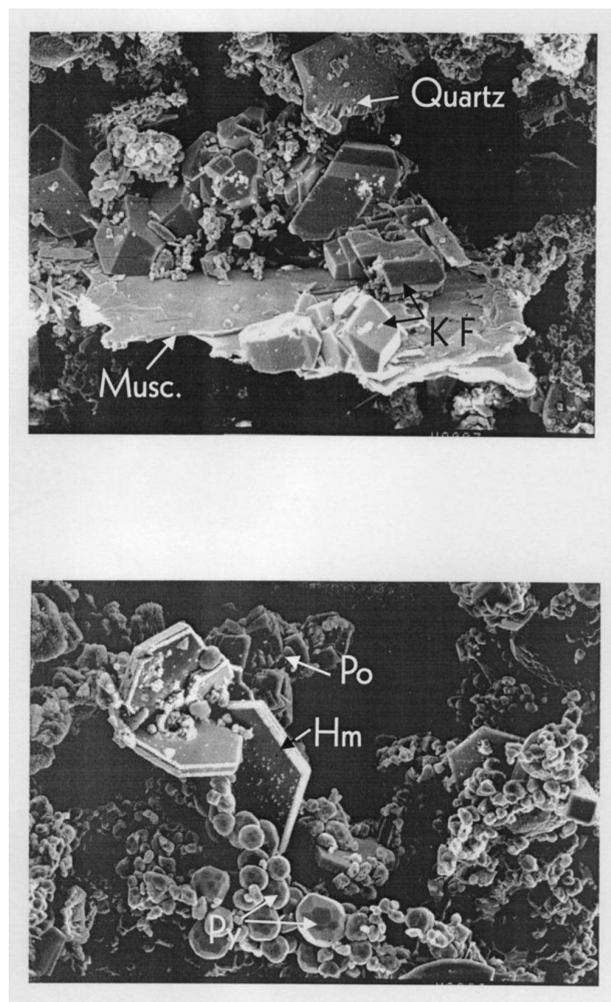

Fig. 1. SEM photomicrographs of the buffer mineral assemblages buffers after experiment (Py = pyrite; Po = pyrrhotite, Hm = Hematite; Musc. = muscovite; KF = potassium feldspar).

morphic morphologies without armoured textures. The KCl solution was prepared by adding the desired amounts of KCl (99.999%, Trem Chemicals Co.) to distilled water. To avoid the problem of relatively slow reaction kinetics of the pH buffer, the starting solution was slightly acidified by adding HCl (5 $10^{-4}m$) close to the pH value expected at a high temperature and pressure. The buffers were placed in a pierced gold tube (diameter = 0.7 cm) which acted as the gold source and buffered the gold activity.

2.4. Sampling Procedure

When the Ti sampling valve is opened, the fluid from the Ti reaction cell flows through a Ti filter placed at the top of the cell into the Ti sampling tube and finally out of the valve into a sample receiver (plastic syringe with titanium and teflon plunger) which is cooled by nitrogen and ice. Simultaneously, a high pressure pump delivers water to the pressure vessel, thereby maintaining the pressure of the system at the desired value. Thus, fluid samples were withdrawn from the Ti reaction cell at essentially constant temperature and pressure, thereby minimising quench problems. A first aliquot, approximately 1 mL, was either discarded or used for pH measurements. About 4 mL were then sampled and prepared for gold analysis. Approximately 0.5 mL of this solution was evaporated onto an aluminium sheet for neutron activation analysis (NAA) with Ge and Ge-Li detectors, and approximately 1–2 mL were diluted for ICP-MS (VG Plasmaquad PQ2+) or ICP (JY
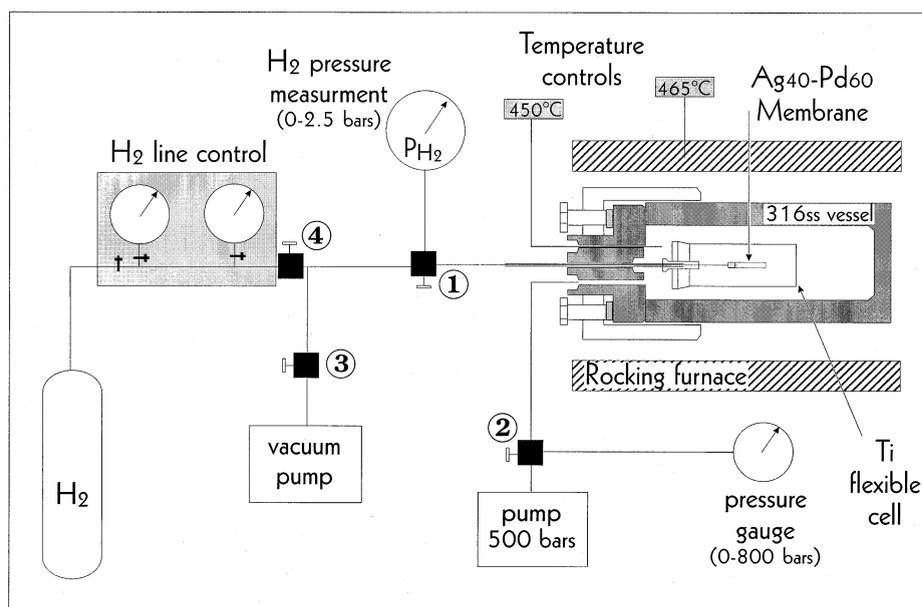
Fig. 2. A schematic diagram of the complete experimental system for the fH$_2$ control test using the semi-permeable membrane technique. 1–3 indicate valves used during fH$_2$ control tests, valve 4 was used during sampling in the solubility experiments. During the solubility runs the membrane and the connections were exchanged for a Ti sampling tube.

38+) analysis. A gold-bearing standard solution was prepared using two titrated Au standard solutions (Titrisol, Merck Co.; Normex, Carlo Erba Co.) and the same KCl as that used in the experiments. The remaining solution was used up to detect the presence of any Sr, by flame absorption spectrometry, to test for the possible contamination of the experimental solution during sampling.

2.5. f H$_2$ Control

The control of redox conditions is critical in this study. The semi-permeable membrane technique (Shaw, 1963) was used to test the behaviour of hydrogen in the titanium reaction-cell system under our experimental conditions. Due to the relatively low temperatures of our experiments ($\leq$ 500°C) an Ag40-Pd60 composition was selected for the membrane, which corresponds to composition with a relatively high permeability in the Ag-Pd system (Gunter et al., 1987). The Ag-Pd tube (thickness 0.2 mm, id 2.5 mm, length 40 mm) filled with rounded quartz grains (natural sand, 0.5 mm) was silver brazed (Hewitt, 1978) on a 1/16″ stainless-steel high-pressure capillary. This capillary was inserted into, and silver brazed on a ¼″ high pressure tube which was used instead of the Ti sample tube in the hydrogen test experiments. The membrane was connected through the capillary to a pressure controller (0–2.5 bars), an H$_2$ reservoir and a vacuum pump. Figure 2 shows the arrangement of the experimental apparatus. Before starting the experiment, the H$_2$ line was air-evacuated by opening valves 1 and 3 (Fig. 2). Two types of experiments were performed.

The first set of experiments was carried out without the Ti flexible cell in order to determine the intrinsic fH$_2$ and fO$_2$ values of the 316SS vessel pressurized with H$_2$O. The results show that at 500 bars, the vessel imposed an intrinsic fH$_2$ of 0.25 bar at 400°C and of 0.20 bar at 500°C and that a steady-state equilibrium was reached after 6 days at 400°C. Theore, 316SS vessels pressurized with water impose an intrinsic fO$_2$ close to the Ni-NiO buffer.

The second set of experiments was designed to test the hydrogen permeability of the Ti cell filled with distilled water by removing (procedure 2a) or by injecting (procedure 2b) hydrogen into the system through the membrane. First, the system was brought to 400°C and 500 bars for 7 days so that the fH$_2$ outside the Ti cell is that imposed by the vessel. Then, hydrogen (~0.26 bar) was introduced into the Ti cell by a repetition of rapid drops and rises in total pressure, allowing contamination of the Ti cell by the external fluid. The membrane was then connected to the vacuum pump and H$_2$ was removed from the Ti cell through the H$_2$ membrane. Four H$_2$ evacuation experiments of increasing duration (P1 to P4, Fig. 3a) were performed and the evolution of the H$_2$ pressure in the membrane was monitored after each evacuation step (Fig. 3a). After the initial drop in H$_2$, the H$_2$ pressure in the membrane rapidly increased and reached in all the case a steady state equilibrium value which could be maintained for duration up to 50 hours without any noticeable diffusion of hydrogen from the vessel to the membrane through the titanium capsule, even at very low fH$_2$ (0.04 bar, Fig. 3a). In procedure 2b, the membrane was connected to the H$_2$-reservoir and three successive injections of H$_2$ (at P$_{H_2}$ ~ 2.4 bars each) were made into the H$_2$ line and the Ag-Pd membrane (I1 to I3, Fig. 3b). Between two injections, the membrane pressure rapidly decreased to a steady-state value which after the second injection, exceeds the intrinsic fH$_2$ of the vessel, indicating that H$_2$ progressively fills the Ti cell. In conclusion, these experiments show that there is no evidence for any significant transfer of H$_2$ by diffusion through the Ti cell either from the Ti cell to the external fluid or the opposite. The data are also inconsistent with the formation of Ti-hydrides, a possibility that needs to be considered given the reported capacity of Ti to absorb large amounts of hydrogen (Lewkowicz, 1996). Thus, the relatively thick, surface oxidized, Ti cell used in this study can be considered to behave like a container closed to hydrogen in our experiments.

An additional fH$_2$ test was performed in a Ti cell filled with 0.5 m KCl solution together with the Py-Po-Mt and the Qtz-KF-Musc buffers (Gibert et al., 1993). In agreement with the result of Kishima (1989) on Py-Po-Mt, this experiment confirmed the relatively fast reaction rates of this assemblage since near equilibrium fH$_2$ values were approached in less than 3 days. However examination of the H$_2$ membrane after the experiment revealed an intense sulfidization of the Ag-Pd alloy which may have raised the fH$_2$ and makes this experimental test inconclusive.

3. RESULTS AND DISCUSSION

3.1. Gold Solubility Measurements

The experimental data are presented in Table 1. The measured solubility of gold in equilibrium with both Py-Po-Mt and Qtz-KF-Mus buffers at 500 bars is 52 ppb $\pm$ 8 ppb at 350°C, 134 $\pm$ 17 ppb at 400°C and 496 $\pm$ 37 ppb at 450°C. Approach

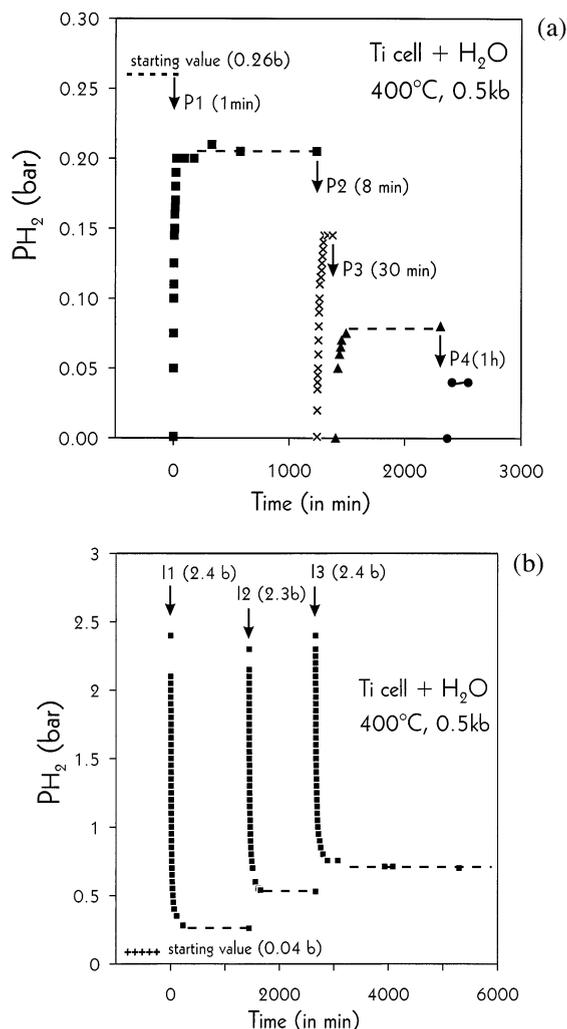2934 F. Gibert, M.-L. Pascal, and M. Pichavant

Fig. 3. Hydrogen permeability test of the Ti cell by removing (4a) or by injecting (4b) hydrogen in the system through the membrane. In procedure (a) H_2 was removed out of the Ti-cell by opening valves 1 and 3 to connect the vacuum pump. From a starting value of 0.26 bar (see text) four time-increasing H_2 removing are performed (P1, one minute; P2, 8 min; P3, 30 min; P4, 60 min) and between each of them the valve 3 is closed and the return of hydrogen in the H_2 membrane was monitored by the H_2 pressure gauge. In procedure (b) H_2 was injected in the Ti cell through the membrane by opening valves 4 and 1. Three successive injections of H_2 (at about 2.4 bar each) were done into the H_2 line and the Ag-Pd membrane (I1 to I3). Between the injections the valve 4 is closed, and the loss of hydrogen in the H_2 membrane was monitored by the H_2 pressure gauge.

of equilibrium from both undersaturation and supersaturation demonstrates that these data represent equilibrium values. An example of this reversibility at 400°C and 500 bars is given in Fig. 4. Supersaturation was obtained by first keeping the temperature at 450°C for 10 days (until steady-state was reached) and then decreasing it to 400°C. In all studied cases, the equilibrium Au concentration was obtained in less than 4 days. When the solutions are buffered with Py-Mt-Hm and Qtz-KF-Mus, the solubility of gold increases to 198 ± 9 ppb at 400°C and 692 ± 10 ppb at 450°C.

Results from NAA analyses correlate with results from ICP-MS or ICP analyses although they are about 20% higher

(Fig. 5). This systematic difference cannot be due to either the precision in weighing the amounts of evaporated solutions for NAA analyses or to the two standard Au solutions used. As ICP-MS and ICP methods gave similar results, these values were preferred to those from the neutron activation analyses. Due to the low gold concentration ($\log(m_{Au}) < -6.5$) in the 350°C runs (Table 1), only the NAA analysis could be used. This may lead to a 20% over-estimation of the gold solubilities at this temperature.

3.2. Analysis and Interpretation of Data

From the literature data and the calculations performed to define the experimental conditions, we can expect that the dominant complexes in our solutions are $Au(HS)_2^-$, $AuCl_2^-$, and a neutral species $HAu(HS)_2^\circ$ or $AuHS^\circ$. The reaction representing the dissolution of gold in an H_2S-bearing aqueous solution can be written in a general form

$$xAu_{(s)} + yH_2S_{(aq)} + zHS^- = Au_x H_{(2y+z-x)} S_{y+z}^{-z} + \frac{x}{2} H_{2(g)}$$
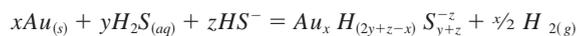
The specific reactions which are important in our study include

$$Au_{(s)} + H_2S_{(aq)} + HS^- = Au(HS)_2^- + \frac{1}{2} H_{2(aq)} \quad (R8)$$

$$Au_{(s)} + 2H_2S_{(aq)} = HAu(HS)_2^\circ + \frac{1}{2} H_{2(aq)} \quad (R9)$$

$$Au_{(s)} + H_2S_{(aq)} = AuHS^\circ + \frac{1}{2} H_{2(aq)} \quad (R10)$$

for bisulfide gold species, and

$$Au_{(s)} + 2Cl^- + H^+ = AuCl_2^- + \frac{1}{2} H_{2(aq)} \quad (R11)$$

for chloride species.

The contribution of $Au(HS)_2^-$ to the measured gold content can be calculated using the equilibrium constant ($\log K$) of reaction R8, determined as -1.35 ± 0.11 at 350°C and 500 bars by Benning and Seward (1996). Using a value of -1.3 (see further discussion) will, therefore, maximize the importance of the $Au(HS)_2^-$ species. Thermodynamic data for $AuCl_2^-$ are given by Zotov and Baranova (1989).

The following seventeen species are considered for the calculation of the gold content in a 0.5 m KCl aqueous solution in equilibrium with Qtz-KF-Mus and Py-Po-Mt buffers at 350°C and 500 bars: $Au(HS)_2^-$, $AuCl_2^-$, KCl°, KOH°, KHS°, K^+, $FeCl_2^\circ$, $FeCl^+$, Fe^{2+}, HCl°, H^+, OH^-, Cl^-, HS^-, $H_2(aq)$, $H_2(g)$, and $H_2S(aq)$. Seventeen equations are required to determine the composition of the solution. They include the expressions of the equilibrium constants for eleven association reactions listed in Table A1 (R8, R11, R12, R13, R16, R17, R18, R19, R20, R21, and R22), the charge balance constraint, and the mass balance equation for chlorine. The last four equations are imposed by the equilibrium with the mineral assemblage which constrains fH_2, aH_2S, aFe^{2+}/a^2H^+, and aK^+/aH^+. Ionic activity coefficients are calculated according to Helgeson et al. (1981), assuming $\gamma_i^{2+} = \gamma_i^{2-} = \gamma Ca^{2+}$ and $\gamma_i^+ = \gamma_i^- = \gamma Na^+$; in accordance with the values of γH_2S recently measured in an H_2O-NaCl solution at low ionic strength by Suleimenov and Krupp (1994), the activity coefficient for the neutral species is assumed to be unity. The system of equations was solved using a Newton-Raphson algorithm, the consistency between activity coefficients and ionic strength being obtained through an iter-

Table 1. Experimental solubility data in KCl (0.5 m) at 500 bars.

Py-Po-Mt and Qtz-KF-Mus buffers — log K_{R10}

| | | | | Calculated | | | | Measured | | | | log K_{R10} |
| | | Sample | Duration* | | | | | NAA | ICP | ICP-MS | | |
Run	°C	number	day	log (H₂)	log(aH₂S)	I	pH	ppb Au	ppb Au	ppb Au	log (m Au)	
1	350											
	350	1	6.5	−1.04	−1.96	0.35	4.54	63.7			−6.49	
	350	3	8.5	−1.04	−1.96	0.35	4.54	45.5			−6.64	
	350	4	10.5	−1.04	−1.96	0.35	4.54	47.6			−6.62	
	350	6	13.5	−1.04	−1.96	0.35	4.54	62.5			−6.50	
	350	7	13.5	−1.04	−1.96	0.35	4.54	47.4			−6.62	−5.18
	350	8	13.5	−1.04	−1.96	0.35	4.54	45			−6.64	−5.20
	350	10	15.5	−1.04	−1.96	0.35	4.54	53			−6.57	−5.13
2	400											
	400	11	8.5	−1.00	−1.4	0.30	4.66	141			−6.15	−5.25
	400	12	14.0	−1.00	−1.4	0.30	4.66	162	145		−6.13	−5.23
	400	13	21.0	−1.00	−1.4	0.30	4.66	176	135		−6.16	−5.26
3	450											
	450	14	11.5	−1.00	−0.78	0.14	5.12	734		496	−5.60	−5.32
	450	15	16.5	−1.00	−0.78	0.14	5.12	631		461	−5.63	−5.35
	450	16	19.5	−1.00	−0.78	0.14	5.12	646	427	480	−5.61	−5.33
4	450											
	450	17	6.5	−1.00	−0.78	0.14	5.12	630	546		−5.56	−5.28
	450	18	10.5	−1.00	−0.78	0.14	5.12	722	472	485	−5.61	−5.33
	450	19	13.5	−1.00	−0.78	0.14	5.12	809	507		−5.59	−5.31
5	450											
	450	20	1.0	−1.00	−0.78	0.14	5.12	405	320	360	−5.74	
	450	21	2.0	−1.00	−0.78	0.14	5.12	396	268	318	−5.79	
	450	22	3.0	−1.00	−0.78	0.14	5.12	550	342	436	−5.65	−5.37
6	400											
	400	23	1.5	−1.00	−1.4	0.30	4.66	78		61	−6.51	
	400	24	2.5	−1.00	−1.4	0.30	4.66	168	101	112	−6.25	
	400	25	4.5	−1.00	−1.4	0.30	4.66	130		117	−6.23	−5.33
	400	26	5.5	−1.00	−1.4	0.30	4.66	124		110	−6.25	−5.35
	400	27	8.5	−1.00	−1.4	0.30	4.66	143		122	−6.21	−5.31
→	450		8.5			0.14	5.12					
→	400		2.0									
	400	28	0.5	−1.00	−1.4		4.66	371		299	−5.82	
→	332	29**	0.0					109				
7	450											
	450	30	6.5	−1.00	−0.78	0.14	5.12	696		556	−5.55	−5.27
	450	31	8.5	−1.00	−0.78	0.14	5.12	601		501	−5.59	−5.31
→	400		10.5									
	400	32	2.0	−1.00	−1.4	0.30	4.66	227		163	−6.08	
	400	33	4.0	−1.00	−1.4	0.30	4.66	184		144	−6.14	−5.24
Py-Hm-Mt and Qtz-KF-Mus buffers												
8	450											
	450	34	3.50	−1.76	−1.04	0.14	5.12			702	-5.45	−5.29
	450	35	5.50	−1.76	−1.04	0.14	5.12			682	−5.46	−5.30
→	400		5.50									
	400	36	6.00	−1.86	−1.68	0.30	4.66			206	−5.98	−5.23
	400	37	9.00	−1.86	−1.68	0.30	4.66			186	−6.02	−5.27
9	400											
	400	38	4.50	−1.86	−1.68	0.30	4.66			196	−6.00	−5.25
	400	39	10.50	−1.86	−1.68	0.30	4.66			204	−5.98	−5.23

* Duration since last temperature change
** Sampled during a break of the pressure capillary and a temperature shutdown, reported has an indicative value only.
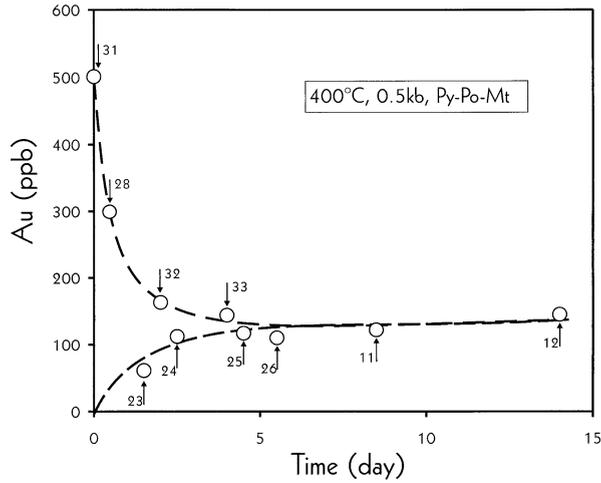 $AuHS° + ½ H_2(g) = Au(s) + H_2S(aq)$ (R10)
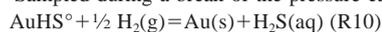
Fig. 4. Gold solubility as a function of time (in day) showing the approach to equilibrium from under- and supersaturation at 400°C, 500 bars.

ative method. As expected, the calculation at 350°C and 0.5 kbar with the Py-Po-Mt buffer shows that $AuCl_2^-$ can be neglected in our experiments while the calculated contribution of $Au(HS)_2^-$ is about 5 ppb. This leads to the conclusion that species other than $Au(HS)_2^-$ or $AuCl_2^-$ control the solubility of gold.

In the literature (e.g., Renders and Seward, 1989; Seward, 1984; Hayashi and Ohmoto, 1991), it is usually accepted that a neutral species such as $AuHS°$ or $HAu(HS)_2°$ can be present in near neutral to slightly acid solutions. From reaction R9 and R10, the variations of gold solubility with aH_2S and fH_2 can be expressed as:
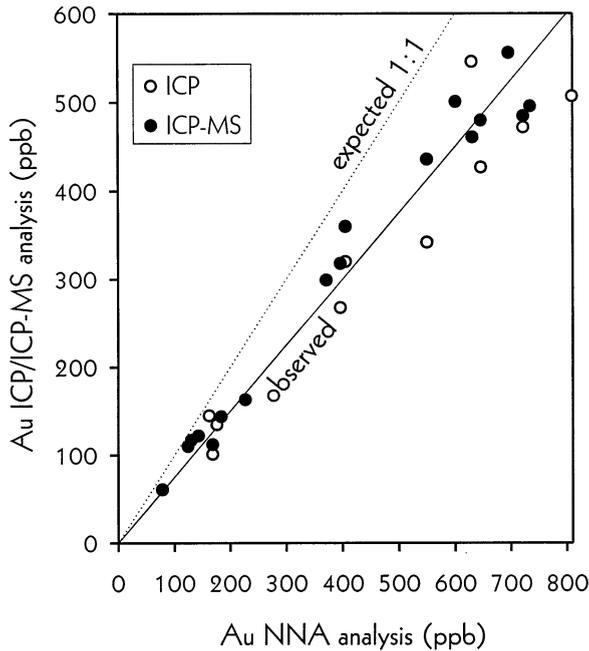

Fig. 5. Comparison between NAA analysis vs. ICP or ICP-MS gold analysis.

$$d\log aHAu(HS)_2° = 2 \, d\log aH_2S - \tfrac{1}{2} \, d\log fH_2 \quad \text{(a)}$$

and

$$d \log aAuHS° = d\log aH_2S - \tfrac{1}{2} \, d\log fH_2 \quad \text{(b)}$$

For the pyrite-magnetite equilibrium

$$\tfrac{1}{2}Fe_3O_4 + 3H_2S = 3/2FeS_2 + 2H_2O + H_2 \quad \text{(c)}$$

we have

$$d\log fH_2 = 3d\log aH_2S \quad \text{(d)}$$

Substituting Eqn. d in Eqns. a and b results in

$$d\log aHAu(HS)_2° = 1/6d \, \log fH_2 \quad \text{(e)}$$

and

$$d\log aAuHS° = -1/6 \, d\log fH_2 \quad \text{(f)}$$

for the variations in gold solubility along the pyrite-magnetite join. When $\log fH_2$ decreases from −1 (Py-Mt-Mt buffer at 400 and 450°C) to −1.86 (Py-Mt-Hm buffer at 400°C) or to −1.76 (at 450°C) the gold solubilities increase of gold solubility from 134 to 198 at 400°C and from 496 to 692 at 450°C. Consequently the $HAu(HS)_2°$ stoichiometry can be ruled out in our experiments.

A similar relation can be found for the variations in $Au(HS)_2^-$ along the Py-Mt join from reaction R8:

$$d\log aAu(HS)_2^- = 1/6 \, d\log fH_2 + d\log aH^+ \quad \text{(g)}$$

For two solutions in equilibrium with the two mineral buffer assemblages (Py-Po-Mt + Qtz-KF-Mus, and Py-Mt-Hm + Qtz-KF-Mus), the pH has a constant value of 4.66 at 400°C and 5.12 at 450°C (Table 1); i.e., $d\log aH^+ = 0$. It follows that (1) $Au(HS)_2^-$ cannot account for the observed increase of gold solubility from Py-Po-Mt to Py-Mt-Hm buffer, and (2) in agreement with the calculations, $Au(HS)_2^-$ is a minor species in our experimental conditions.

If $AuHS°$ is the dominant species in our experiments, ($\log mAu + \tfrac{1}{2} \log fH_2$) should be positively correlated with $\log aH_2S$ (reaction R10); the slope of the correlation line defines the Au/S ratio of the species. Results are given in Fig. 6 for the two redox buffers at 400°C and 450°C and for the measured equilibrium data. In this figure, the experimental data yied slopes close to unity which is the expected slope for the $AuHS°$ species (a slope of +2 is would suggest the presence of the $HAu(HS)_2°$ species). This clearly demonstrates that the main gold-bearing species in our experiments is $AuHS°$. The derived thermodynamic data for $\log K_{R10}$ are given in Table 2 for each individual experiments.

3.3. Comparison with Previous Literature Data

3.3.1. AuHS° vs. HAu(HS)₂° dominant species

Two previous studies have shown the importance of neutral bisulfide gold-bearing species at high temperatures. Hayashi and Ohmoto (1991) have suggested the $HAu(HS)_2°$ stoichiometry from experiments in ($NaCl + H_2S$) aqueous solutions at 250–350°C and Psat. The critical parameters of these experiments (i.e., aH_2S, fH_2, fS_2) were controlled by the sulfur
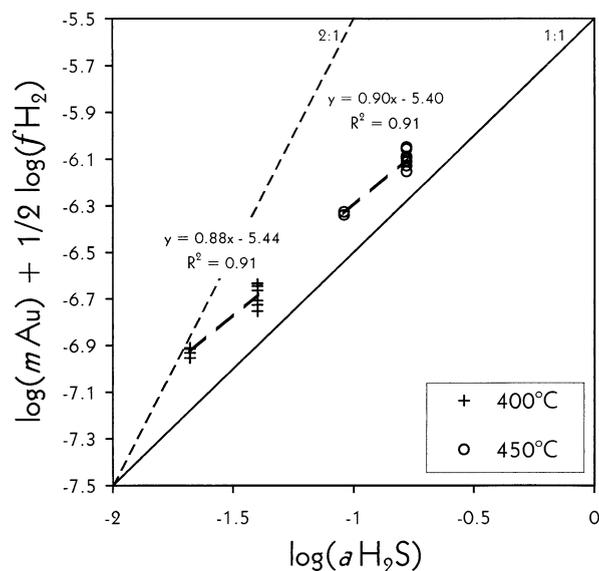
Fig. 6. Stoichiometry plot for neutral gold species at 450 and 400°C using Eqns. R9 and R10. Data points represent individual samples in which equilibrium is reached. At each temperature the slope for the experimental data points is close to 1, demonstrating that AuHS° species is the dominant gold-bearing species in the experimental solution.

hydrolysis reaction and the sulfide/sulfate reaction. Because of (1) the uncertainty in measuring the volume of silica tubes, (2) the poor correlation of experimental results in a $\log(aH_2S)$ vs. $(\log m_{Au} + \frac{1}{2} \log fH_2)$ plot (Hayashi and Ohmoto, 1991, Fig.

Fig. 7. Comparison of the equilibrium constants for AuHS° species (reaction R10) plotted as a function of temperature at 500 bars pressure. Note that Hayashi and Ohmoto (1991) data have been reinterpreted in terms of AuHS°.

5) and (3) the fact that, according to the authors, the $Au(HS)_2^-$ content can be neglected in their experiments, the data of Hayashi and Ohmoto (1991) can be better interpreted in terms of AuHS° (Gibert et al., 1993, Fig. 4). We can see in Fig. 7 that

Table 2. Selected fugacities and activities used in this study

	350°C P_{sat}	350°C 0.5 kb	400°C 0.5 kb	450°C 0.5 kb	Data source
Quartz-K-Feldspar-Muscovite buffer					
aK^+/aH^+	3.57	3.66	3.57	3.47	1
Py-Po-Mt buffer					
$aFeS$	0.5	0.5	0.5	0.5	2
Log (fS_2)	−8.86	−8.83	−7.05	−5.52	1
Log (fS_2)	−8.94	−8.94	−7.19	−5.68	3
Log (fS_2)	−9.15	−9.15	−7.37	−5.78	4
Log (fS_2)	−8.69	−8.69	−7.04	−5.61	2
Log (fS_2)	−8.89	−8.89	−7.14	−5.64	5
Log (fO_2)	−29.34	−29.33	−26.00	−23.14	1
Log $(fO_2) \pm 0.05$	−29.38	−29.38	−26.01	−23.09	3
Log (fH_2)	−1.11	−1.04	−1.00	−1.00	1
Log (fH_2)		−1.03	−1.04	−1.05	3
Log aH_2S	−1.88	−1.96	−1.40	−0.78	1
Log (fH_2S)		−0.49	−0.12	0.19	1
Log (fH_2S)		−0.53	−0.16	0.11	3
aFe^{2+}/aH^{+2}	2.53	2.61	2.34	2.84	1
Py-Hm-Mt buffer					
Log (fO_2)	−27.40	−27.38	−24.30	−21.62	1
Log (fS_2)	−7.57	−7.53	−5.92	−4.51	1
Log (fH_2)	−2.08	−2.01	−1.86	−1.76	1
Log aH_2S	−2.21	−2.28	−1.68	−1.04	1
aFe^{2+}/aH^{+2}		2.29	2.06	2.58	1

Sources: 1 SUPCRT92, Johnson et al. (1992); 2. Scott and Barnes (1971); 3. Kishima (1989); 4. Toulmin and Barton (1964); 5. Barton and Skinner (1979).

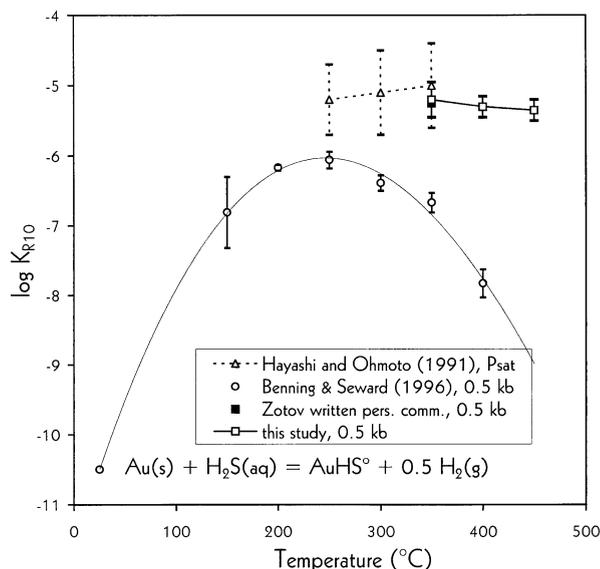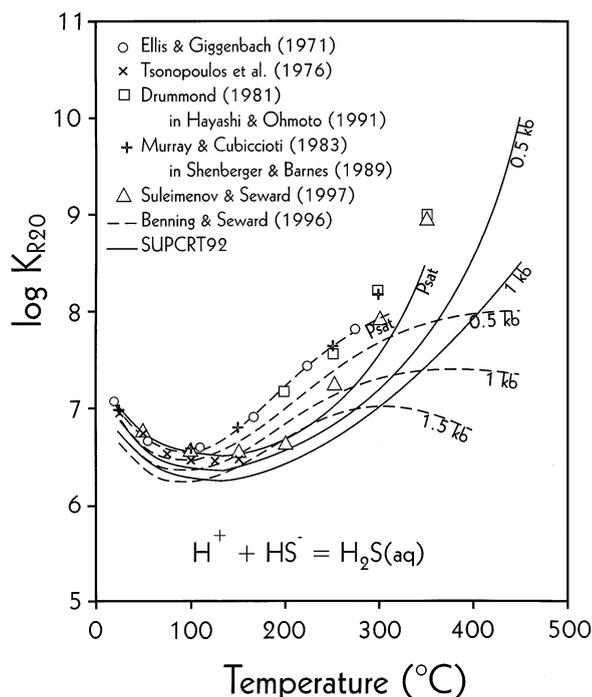Fig. 8. Comparison of values of the dissociation constant of $H_2S(aq)$ ($\log K_{R20}$) used by Benning and Seward (1996) and those used in this study (SUPCRT92). Figure shows also the available experimental data sets (see text) and some other data used in the literature.

Table 3. Effect of change in log K_{R20} on computed gold solubility and speciation

Reactions:					log K
$Au(s) + HS^- + H_2S(aq) = Au(HS)_2^- + .5\ H_2(g)$					-1.03
$Au(s) + H_2S(aq) = AuHS° + .5\ H_2(g)$					-6.06
$O_2(g) + .5\ H_2(g) = H_2O$					20.13
$H^+ + OH^- = H_2O$					10.90
$HS^- + H^+ = H_2S(aq)$					—
$H_2(g)$					-1.824

$\Sigma m\ S = 2\ mAu(HS)_2^- + mAuHS° + mH_2S(aq) + mHS^- = 0.1094$
$mHS^- + mOH^- + mAu(HS)_2^- = mH^+$

$T = 250°C$			$HS^- + H^+ = H_2(aq)$		$(R20)$	
$P = 0.5$ kb			$\log K_{R20} = 7.36$		$\log K_{R20} = 6.82$	
i	$\log (a_i)$	m_i		$\log (a_i)$	m_i	
$Au(HS)_2^-$	-5.25	$5.71E-6$	1125 ppb	-4.98	$1.07E-05$	2102 ppb
$AuHS°$	-6.10	$7.86E-7$	155 ppb	-6.11	$7.85E-7$	155 ppb
$H_2S(aq)$	-0.96	$1.09E-1$		-0.96	$1.09E-1$	
OH^-	-6.75	$1.79E-7$		-7.03	$9.55E-8$	
H^+	-4.14	$7.37E-5$	pH = 4.14	-3.87	$1.39E-4$	pH = 3.87
HS^-	-4.18	$6.78E-5$		-3.90	$1.28E-4$	
fH_2	-1.83			-1.83		
fO_2	-19.21			-19.21		
$\log (\gamma^{1+})$		$-7.45E-3$			$-1.02E-2$	
I		$7.37E-5$			$1.38E-4$	

our data for 350–450°C and 500 bars are in good agreement with both the reinterpreted data from Hayashi and Ohmoto (1991) at 250–350°C and Psat and the unpublished point of Zotov at 350°C, 500 bars (log $K_{R10} = -5.25 \pm 0.15$; written pers. commun.).

Benning and Seward (1996) have also indicated the presence of the AuHS° species at T = 150–450°C and P = 0.5–1.5kbar. In spite of the agreement with our study in terms of the stoichiometry of the neutral gold-bearing species, the equilibrium constants derived by Benning and Seward (1996) are up to two log units lower than ours (Fig. 7). For these authors two reasons might explain this discrepancy: (1) uncertainties in the thermodynamic data for the Py-Po-Mt mineral buffer and (2) the choice of different ionization constant of $H_2S(aq)$. Below we explore in details these two possible explanations.

3.3.2. The Py-Po-Mt redox buffer

In this study, we have used the thermodynamic data for Py-Po-Mt from the SUPCRT92 database assuming an activity of 0.5 for the FeS component in pyrrhotite (Scott and Barnes, 1971). This activity value is similar to those derived by Barker and Parks (1986). The calculated values of fS_2 using SUPCRT92 (Table 2) agree with the SUPCRT92-independent values given by Kishima (1989). The literature fS_2 values in the range 350–450°C (Toulmin and Barton, 1964; Scott and Barnes, 1971; Barton and Skinner, 1979) are in good agreement with one another, except the older data of Toulmin and Barton (1964) at 350°C. The comparison of the three more recent studies (Kishima, 1989; Scott and Barnes, 1971; Barton and Skinner, 1979) give small variations of fS_2: 0.25 at 350°C, 0.15 at 400°C, and 0.07 at 450°C. Thus, the uncertainty on fS_2 is small in the temperature interval of 350–450°C. According to Kishima (1989), the uncertainty of fO_2 calculated from the literature data, may be higher: ± 0.23 at 327°C. This uncer-

tainty on oxygen fugacity may lead to a small uncertainty of fH_2 and of aH_2S through reactions R1, R2, and R4 (Table A1). However, taking high values of fO_2 would induce low values of fH_2 and of aH_2S and vice versa. As a consequence, the uncertainty on $(½ \log(fH_2) - aH_2S)$ is likely to be small. Furthermore, Kishima (1989) measured fH_2 and fH_2S in equilibrium
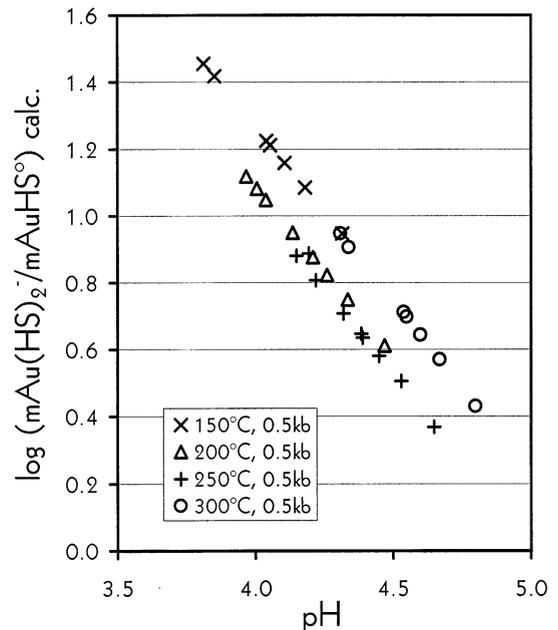

Fig. 9. Log($mAu(HS)_2^-/mAuHS°$) ratios in the experiments of Benning and Seward (1996) at pH ~ 4 computed using their equilibrium constant data base. $Au(HS)_2^-$ is expected to be 2.5–30 times more important than AuHS°. Note that in Benning and Seward (1996) experiments aH_2S is strongly decreased while pH is increased.
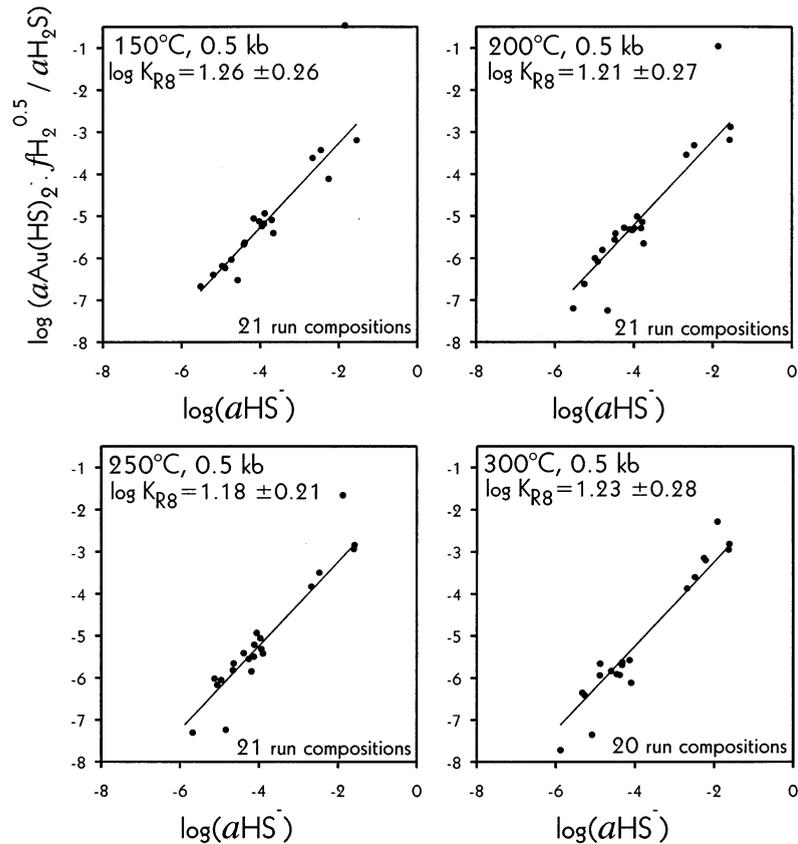
Fig. 10. Stoichiometry plots for $Au(HS)_2^-$ from 150 to 300°C using equations R8 for the Benning and Seward (1996) runs. The slope for the experimental data points at each temperature is close to 1, demonstrating that $Au(HS)_2^-$ species is likely the dominant gold-bearing species in their experimental solutions.

with Py-Po-Mt in the interval of 300–500°C and at pressures below 1 kbar, and derived oxygen fugacities, which to date constitute the most reliable dataset on the Py-Po-Mt buffer under hydrothermal conditions. Table 2 shows the comparison between the fO_2, fH_2, and fH_2S calculated from SUPCRT92 and those measured by Kishima (1989). The differences are always very small (<0.05 for fO_2 and fH_2: <0.08 fH_2S). Therefore, the uncertainty of the Py-Po-Mt buffer cannot explain the observed difference of 2 log units for log K_{R10}.

3.3.1.2 The ionization constant of $H_2S(aq)$

In their study, Benning and Seward (1996) used ionization constant of $H_2S(aq)$ of Seward's (1973) based on a polynomial extrapolation similar to Clarke and Glew (1966) of the Ellis and Giggenbach (1971) experiments. In this work, we use the $H_2S(aq)$ ionization constant based on the data of Barbero et al. (1982) and Tsonopoulos et al. (1976), taken from the SUPCRT92 software (Shock et al., 1989; Johnson et al., 1992). Figure 8 shows the two sets of log K_{R20} values, with other data from the literature. At low temperatures, the ionic association constants are quite similar, and the pressure dependence is in good agreement with the Sretenskaya (1977) data. At higher temperatures, the log K_{R20} values diverge, reaching a difference of up to 2 log units at high temperature and pressure. Recent spectroscopic data from Suleimenov and Seward (1997)

do not show the inversion of curvature predicted by the extrapolation of the Ellis and Giggenbach (1971) data up to 350°C (Fig 8). Since, at constant pressure, a temperature increase results in a large decrease of the dielectric constant (ϵ) of the solution, leading to an increased association, the SUPCRT92 constants for K_{R20} are preferred in this study.

Until a more accurate dataset for the association constant of $H_2S(aq)$ becomes available at high temperature and pressure, the effect of the different choices of log K_{R20} on the derived equilibrium constant of gold-bearing species must be analysed. Table 3 shows the computed speciation for two models where the only variable is the association constant of $H_2S(aq)$. The method of resolution is the same as previously discussed in this paper, and speciation is calculated at 250°C and 500 bars for a pure H_2S solution ($\Sigma S = 0.1094$) equilibrated at 25°C with a pressure of hydrogen of 0.03575 bar (composition of run 4 in Benning and Seward, 1996). The first model uses thermodynamic data from Benning and Seward (1996); in the second one, the association constant of $H_2S(aq)$ is the one we have used (Table A1). The results show that the variation of log K_{R20} affects only the pH, HS$^-$ and $Au(HS)_2^-$ molalities. In contrast, $mH_2S(aq)$ (the dominant sulfur species) and $mAuHS°$ remain almost unchanged (Table 3). Thus, if $H_2S(aq)$ is the dominant sulfur species, the choice of the dissociation constant of $H_2S(aq)$ is not
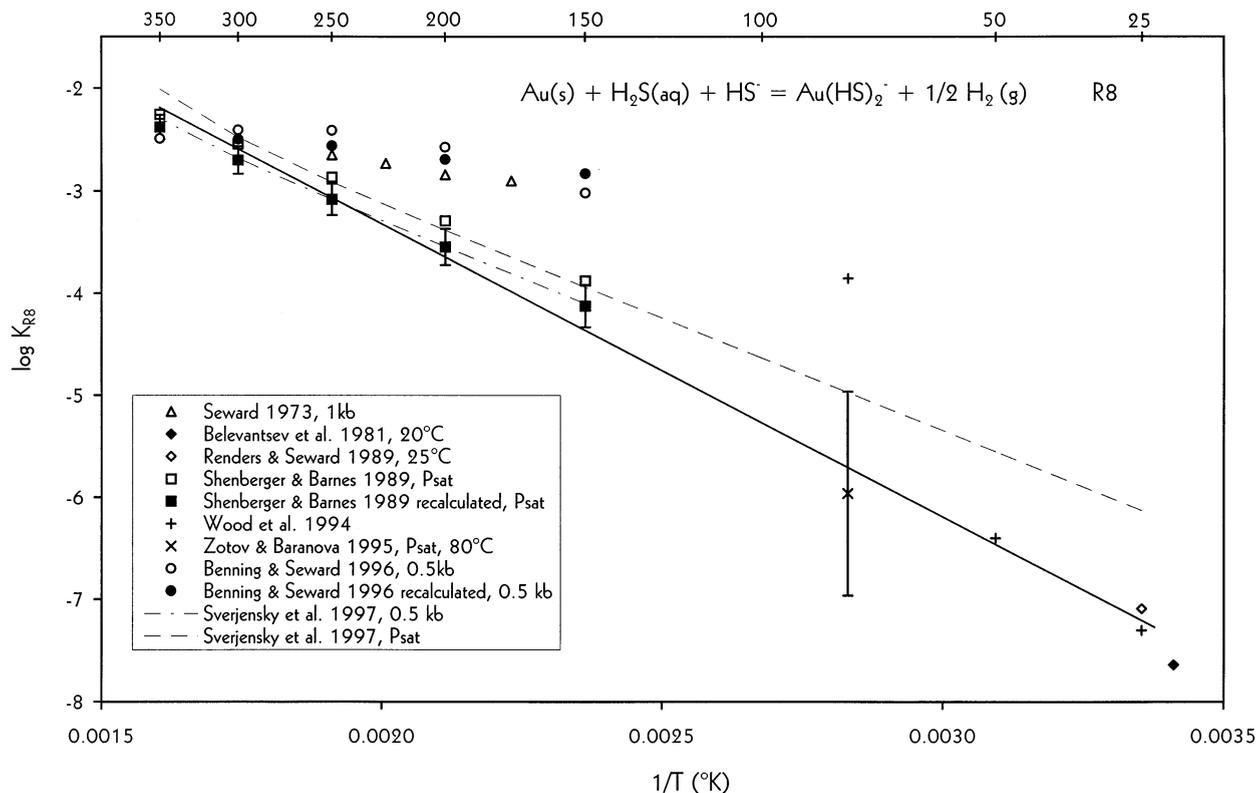
Fig. 11. Equilibrium constant for the reaction $Au(c) + H_2S(aq) + HS^- = Au(HS)_2^- + \frac{1}{2} H_2(aq)$ (R8) recalculated from the experimental data of Shenberger and Barnes (1989). The equilibrium constant show a linear dependence against 1/T up to 350°C at Psat as expected from an pseudo-isocoulombic reaction.

critical in experiments where AuHS° (a neutral species) is the main gold-bearing species. In other words, if AuHS° is the species undergoing a major concentration, the choice of the association constant of $H_2S(aq)$ does not account for the difference in Au solubility between Benning and Seward (1996) and the present study.

3.3.2 Au(HS)$_2^-$ species

Benning and Seward (1996) gave a graphical evidence for the dominance of the AuHS° species, between 150°C and 300°C, in (log $m_{Au,tot}$) vs. (log $m_{S,tot}$) plots for runs with a pH ≈ 4 (Fig. 7, p. 1856 in Benning and Seward, 1996). They then used an independent least-square refinement to derive the equilibrium constants for reactions R8 and R10 (Table 2 in Benning and Seward, 1996). However, the derived constants seem inconsistent with the graphical analysis: for example, using their equilibrium constants, the computed gold speciation in their runs shows that $Au(HS)_2^-$ is twice to thirty times more important than AuHS° at pH ≈ 4 (Table 3 and Fig. 9). Indeed, in a (log $m_{Au,tot}$) vs. (log $m_{S,tot}$) plot, the Au/S ratio of the gold-bearing species is given by the partial derivative of $m_{Au,tot}$ with respect to $m_{S,tot}$ only if, in addition to temperature and pressure, the fH_2 and pH are constant. Benning and Seward (1996) have measured gold solubility in H_2S aqueous solutions ($\pm$NaHS $\pm$ H_3PO_4) and according to these authors, fH_2 may be considered constant in their experiments at pH ≈ 4. However,

Fig. 9 shows that the pH varies by nearly 1 order of magnitude between the data used in their graphical analysis and, therefore, cannot be considered constant. Careful examination of the log $m_{Au,tot}$ vs. log $m_{S,tot}$ plots (Fig. 7, in Benning and Seward, 1996) shows that the low and high pH values correspond to high and low gold concentrations, respectively. This suggests a marked influence of the pH on the gold solubility in their runs at pH ≈ 4, and consequently the presence of a charged species.

If $Au(HS)_2^-$ is dominant in the Benning and Seward (1996) experiments, $(\log(m_{Au,tot}) + \frac{1}{2} \log (fH_2) - \log (aH_2S))$ should be positively correlated with $\log(aHS^-)$ (with a slope of 1). In this type of diagram, the presence of the neutral AuHS° species would be indicated by a horizontal trend (expected at about −6.15 at 150°C to −5.35 at 300°C if the new interpretation of the Hayashi and Ohmoto (1991) data is correct). To allow for a more precise comparison of the different data from the literature we have recalculated the solubility data of Hayashi and Ohmoto (1991), Benning and Seward (1996), Shenberger and Barnes (1989), using the same thermodynamic base. The equilibrium constants used for this calculation are given in Table A1. The results of the recalculated experimental solubility data of Benning and Seward (1996) are plotted in Fig. 10. The best fit lines are close to 1 and clearly demonstrate that $Au(HS)_2^-$ is likely to be the dominant gold-bearing species in most of the Benning and Seward (1996) experiments. Two main consequences follow: (1) surprisingly there is no clear
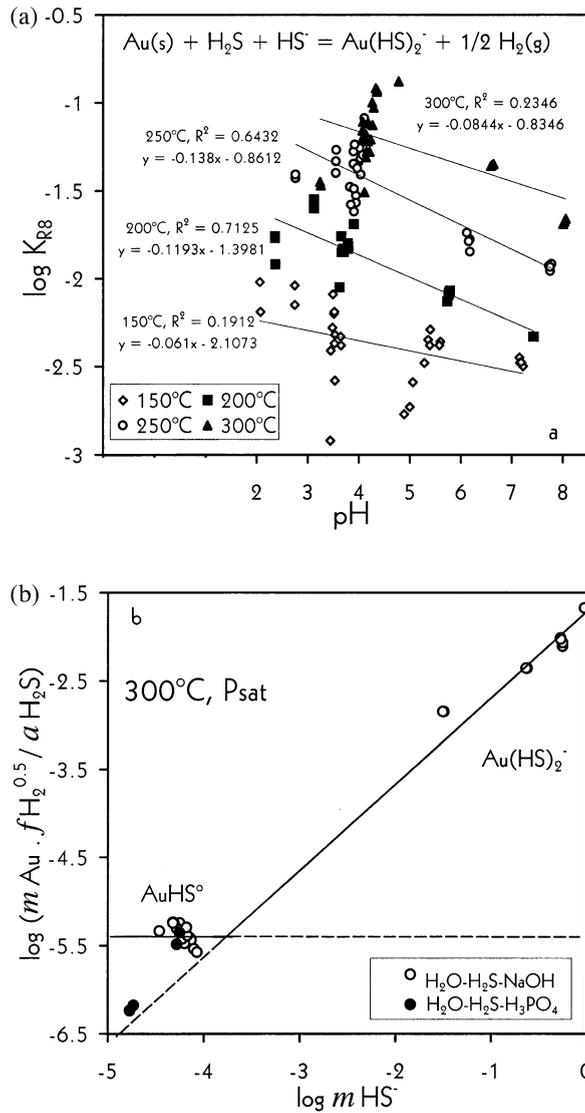
Fig. 12. a. Log K_{R8} values recalculated from the experimental data of Shenberger and Barnes (1989) as a function of pH. b. Stoichiometry plots for $Au(HS)_2^-$ and $AuHS°$ at 300°C for the experimental data of Shenberger and Barnes (1989).

evidence of the presence of the $AuHS°$ species in the experiments of Benning and Seward (1996); and (2) as the $Au(HS)_2^-$ species is dominant in most of their runs, the choice of the values of the dissociation constant of $H_2S(aq)$ is critical to the results of their least-square fit (see previous section). The new values of Log K_{R8} derived from Benning and Seward (1996) data are plotted in Fig. 11 together with the previous ones. For comparison, the recalculated data of Shenberger and Barnes (1989) plotted in Fig. 11, together with other experimental data available on $Au(HS)_2^-$ at an intermediate temperature (Seward, 1973; Zotov and Baranova, 1995) and at a low temperature (Belevantsev et al., 1981; Renders and Seward, 1989; Wood et al., 1994) and with the predicted values of Sverjensky et al. (1997). The calculation has been performed in terms of the reaction

$$Au(c) + H_2S(aq) + HS^- = Au(HS)_2^- + \tfrac{1}{2} H_2(aq) \qquad (R8)$$
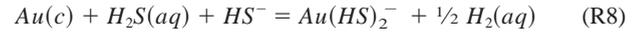
Writing equation R8 with $H_2(aq)$ instead of $H_2(g)$ makes the reaction more symmetrically balanced and keeps its pseudo-isocoulombic properties, inducing an expected $\Delta Cp=0$ (Lindsay, 1980). Consequently, the $\Delta H°_R$ must be roughly constant, so that a plot of (log K) vs. 1/T should be linear. Figure 11 shows that most of the data are in good agreement with each other. In contrast, the Seward (1973) and Benning and Seward (1996) data (both the original data and that recalculated in this study using the Table A1 database) still conflict with the results from Shenberger and Barnes (1989) (see discussion in Zotov and Baranova, 1995 and in Sverjensky et al., 1997). The above calculations and discussion show that this discrepancy is too large to be the result of the choice of a different dissociation constant of $H_2S(aq)$.

The equilibrium constants from Shenberger and Barnes (1989) recalculated with the data base of table A1 are slightly shifted in comparison with the previous ones (no more than 0.2 log unit; Fig. 11). These new recalculated values have probably been slightly over-estimated because the log K_{R8} values, derived by Shenberger and Barnes (1989) for individual runs, exhibit a negative dependence upon the pH (Fig. 12a). This dependence indicates that another gold species becomes more and more important in acidic runs as already suspected by these authors. Figure 12b shows that the Shenberger and Barnes (1989) data seem to be compatible with the $AuHS°$ species, and are in reasonable agreement with a log K_{R10} near -5.1 derived in the present study from the Hayashi and Ohmoto (1991) data.

The reasons for the discrepancy between our results and those of Benning and Seward (1996) are not clear. Pan and Wood (1994) discuss the possibility that the lower gold solubility values in their experiments are due to generation of H_2 in the sampling tube because of the use of a Ti-filter. However, this effect can be totally ruled out in our experiments since the same Ti-filter device was used in this study yet we measured a higher solubility than Benning and Seward (1996). Our new results are in good agreement with the recalculated data of Hayashi and Ohmoto (1991) and with Zotov (written pers. commun.) despite the fact the experimental designs of these three studies are completely different: Hayashi and Ohmoto (1991) used chloride and sulphide-bearing aqueous solutions buffered by a sulphur hydrolysis reaction and sulphate-sulphide equilibrium; Zotov (written pers. commun.) used pH-variable sulfide-bearing aqueous solution with H_2 produced by Al metal; in the present study, we have used Py-Po-Mt and Py-Mt-Hm buffers. Furthermore, the data of Shenberger and Barnes (1989) also seem compatible with the expected presence of the $AuHS°$ species.

3.3.3. Thermodynamic constants

The total contribution of $AuCl_2^-$ and $Au(HS)_2^-$ to the observed gold solubilities in our experiments has been calculated using for $AuCl_2^-$ the thermodynamic constants from Baranova and Zotov (1989) and for $Au(HS)_2^-$ our new stability constants extrapolated from Shenberger and Barnes (1989) (Table A1). At 350°C, 400°C, and 450°C, it was determined to be 5 ppb (0.4 ppb as $AuCl_2^-$ + 4.7 ppb as $Au(HS)_2^-$), 35 ppb (5 ppb as

Table 4. Equilibrium constants for the AuHS° and Au(HS)$_2^-$ species

	AuHS° + ½ H$_2$(g) = H$_2$(aq) + Au(s)					(R10)	
	150°C	200°C	250°C	300°C	350°C	400°C	450°C
P$_{sat}$	5.90§	5.40§	5.20* ± 0.5	5.10* ± 0.5	5.00* ± 0.6		
500 bar	6.15§	5.65§	5.45§	5.35§	5.20† ± 0.25	5.30† ± 0.15	5.40† ± 0.15
	Au(HS)$_2^-$ + ½ H$_2$(g) = H$_2$S(aq) + HS$^-$ + Au(s)					(R8)	
	150°C	200°C	250°C	300°C	350°C	400°C	450°C
P$_{sat}$	2.64‡ ± 0.2	2.14‡ ± 0.2	1.77‡ ± 0.3	1.50‡ ± 0.3	1.34‡ ± 0.2		
500 bar	2.84§	2.25§	1.85§	1.50§	1.30§	1.25§	1.20§

* Recalculated from the data of Hayashi and Ohmoto (1991).
† Calculated from the solubility data of this study.
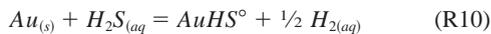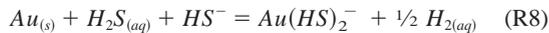‡ Recalculated from the data of Shenberger and Barnes (1989).
§ Interpolated/extrapolated.

AuCl$_2^-$; 30 ppb as Au(HS)$_2^-$), and 117 ppb (41 ppb as AuCl$_2^-$; 76 ppb as Au(HS)$_2^-$) with the Py-Po-Mt buffer. At 400°C and 450°C, it was calculated as 35 ppb (13 ppb as AuCl$_2^-$; 22 ppb as Au(HS)$_2^-$) and 150 ppb (99 ppb as AuCl$_2^-$; 50 ppb as Au(HS)$_2^-$) with the Py-Mt-Hm buffer. Recently Suleimenov and Seward (1997) have given a new determination for the dissociation constant of H$_2$S (Fig. 9) at 20–350°C and Psat. From their study, a new logK$_{R20}$ of -8.28, -9.10, and -10.70 can be extrapolated at 500 bars and 350, 400, and 450°C, respectively. As a consequence, the contributions of the Au(HS)$_2^-$ species in our experiments change to 1.8 ppb at 350°C, 7.3 ppb at 400°C, 17 ppb at 500°C with the Py-Po-Mt buffer and 1.3 ppb at 400°C, 5.4 ppb at 450°C with the Py-Mt-Hm buffer.

Table 4 summarizes the final calculated solubility constants for reactions R8 (Au(HS)$_2^-$) and R10 (AuHS°).
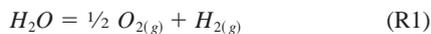
4. GEOLOGICAL APPLICATIONS

Specific reactions important in gold transport and deposition are

$$Au_{(s)} + H_2S_{(aq)} + HS^- = Au(HS)_2^- + ½ H_{2(aq)} \quad (R8)$$

$$Au_{(s)} + H_2S_{(aq)} = AuHS° + ½ H_{2(aq)} \quad (R10)$$

and

$$Au_{(s)} + 2Cl^- + H^+ = AuCl_2^- + ½ H_{2(aq)} \quad (R11)$$

These reactions, combined with the following equilibrium:

$$H_2S_{(aq)} = HS^- + H^+ \quad (R20)$$

$$H_2O = ½ O_{2(g)} + H_{2(g)} \quad (R1)$$
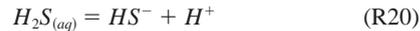
show that, besides temperature and pressure, critical parameters for the mechanisms of gold transport and deposition are the total sulfur (ΣS) and total chloride (ΣCl) concentrations in the solution, the redox state (fO$_2$) and the pH.

A common advocated deposition process is the variation in pH. Using the stability constants summarized in Tables 4 and A1, gold solubility and the relative importance of the two gold-bisulfide complexes (AuHS° and Au(HS)$_2^-$) and the chloride species (AuCl$_2^-$) are compared as the function of pH in a

fluid (H$_2$O-NaCl 0.5m) buffered by the Py-Po-Mt assemblage. The effect of temperature has been investigated from 250°C up to 450°C (Fig. 13). In this system, fO$_2$, fH$_2$, fS$_2$, and consequently aH$_2$S are constant, and the pH is varied by modifying the Cl concentrations. We see that cooling must be an efficient mechanism for gold precipitation. AuCl$_2^-$ is dominant in the acidic region and only for high temperature (>30°C). At lower temperatures (350–250°C), and for pH < 5, AuHS° is dominant, meaning that under these conditions gold will not precipitate due to a change in pH. For pH > 5, Au(HS)$_2^-$ is the dominant gold species and gold can precipitate through neutralization. In this calculation, we note that the aH$_2$S and aH$_2$ values remain constant at a given temperature, while the aHS$^-$ and ΣS values do not. Thus, the observed increase of the
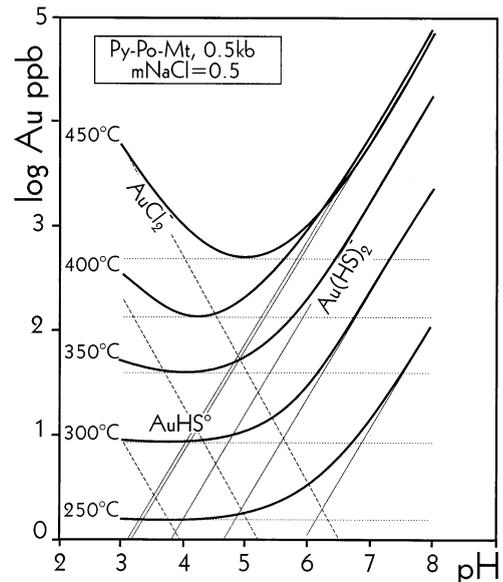
Fig. 13. Solubility contours of gold (ΣAu = mAuCl$_2^-$ + mAuHS° + mAu(HS)$_2^-$; heavy lines) and relative importance of the three gold-bearing species, AuCl$_2^-$ (dashed thin lines), Au(HS)$_2^-$ (thin lines) and AuHS° (dotted thin lines) as a function of temperature (250 up to 450°C) and pH in a fluid (H$_2$O-NaCl 0.5m) buffered by the Py-Po-Mt assemblage.

Fig. 14. Solubility contours for gold ($\Sigma Au = mAuCl_2^- + mAuHS^\circ + mAu(HS)_2^-$) in a solution of T=350°C, 500 bar, $\Sigma S = 0.01$, and $\Sigma Cl = 0.5$, shown as a function of fO_2 and pH.
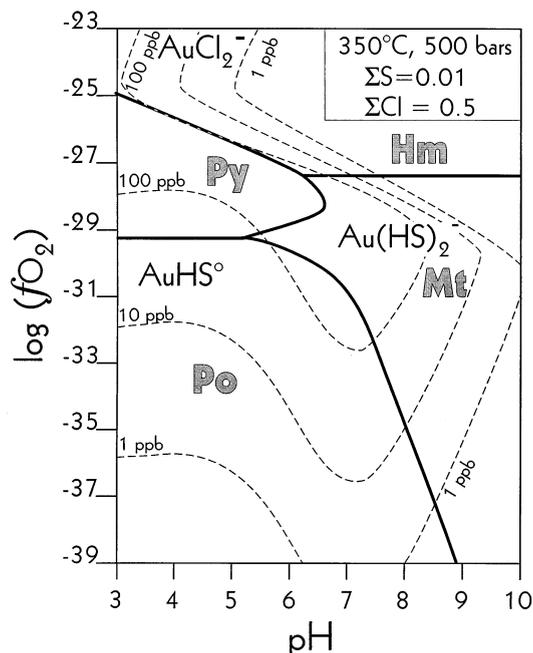
$Au(HS)_2^-$ content in an alkaline solution is not directly due to an increase in pH, but rather in aHS^-.

Typically, gold solubility models are presented in $\log(fO_2)$ vs. pH diagrams calculated for constants values of ΣS and ΣCl (Shenberger and Barnes, 1989; Hayashi and Ohmoto, 1991). Using this diagram, fO_2 and pH variations can be shown to control gold deposition. A diagram of this kind calculated for 350°C, $\Sigma Cl = 0.5$ and $\Sigma S = 0.01$ is presented in figure 14. When $AuCl_2^-$ is the dominant species, an increase in pH is expected to precipitate Au whereas a decrease in pH will cause the deposition of gold if the $Au(HS)_2^-$ species dominates (Fig 14). In the same projection, a decrease in fO_2 is an effective mechanism for gold precipitation regardless of whether gold is transported as chloride or bisulfide complexes. However, we believe that the choice of the $\log(fO_2)$ vs. pH diagram is confusing, because this type of diagram does not take into account the variations of ΣS and moreover, postulates large variations of natural pH. In contrast with chlorine which almost never enters the mineral compositions ($\Sigma Cl = $ constant), S is a main component of minerals such as pyrrhotite, pyrite, arsenopyrite, sphalerite, etc, found in association with gold in natural deposits. The total S content of the gold-bearing solution is controlled by the stabilities of these sulphides and thus ΣS, far from being constant, may undergo major changes through sulfide precipitation. Moreover, the pH of hydrothermal fluids is in nearly all cases determined by equilibrium with silicate minerals (feldspar, micas, etc.) with a value close to neutrality ± 1. Consequently, two other projections are preferred in this study: the $\log(fO_2)$ vs. $\log(aH_2S)$ at constant pH and ΣCl (Hayashi and Ohmoto, 1991) and the $\log(fO_2)$ vs. pH at constant ΣCl and variable ΣS.

The solubility of gold has been computed as a function of $\log(fO_2)$ and $\log(aH_2S)$ at 350°C and 250°C (Fig. 15 a and b).
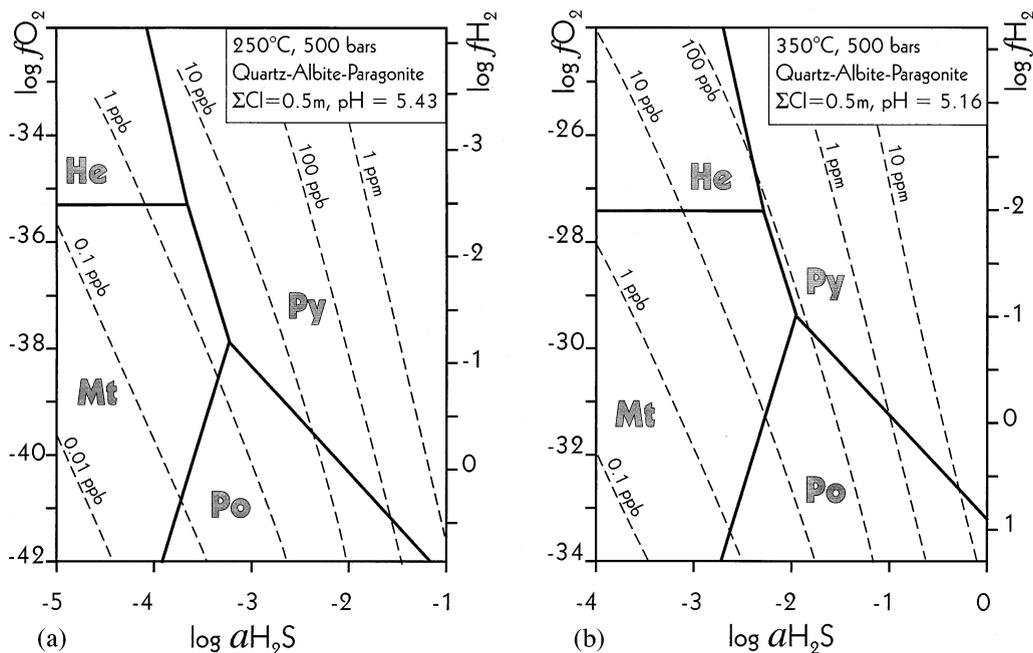
Fig. 15. Calculated solubility of gold at 250°C (a) and 350°C (b), computed as a function of fO_2 and aH_2S(aq) for a 0.5 m NaCl aqueous solution in equilibrium with the quartz-albite-paragonite pH buffer. The dashed lines represent the solubility contours of gold ($\Sigma Au = mAuCl_2^- + mAuHS^\circ + mAu(HS)_2^-$). The solid lines separate the stability fields of pyrite, pyrrhotite, magnetite, and hematite.

Gold solubility was calculated for a NaCl aqueous solution with $\Sigma Cl = 0.5$ m. The pH is controlled by the quartz-albite-paragonite mineral assemblage which is common in the wall-rock of epithermal gold deposits. Also shown in these diagrams are the Py, Po, Mt, and Hm stability fields.

The gold content in economic deposits is typically of the order of a few ppm (Kesler, 1973; Hannington and Scott 1989). For a plausible water/rock ratio of 1000 (Barnes, 1979), mass balance considerations reveal that hydrothermal fluids would have precipitated 10 ppb to obtain a concentration of 10 ppm in mineralized rocks (or 5 ppb for a water-rock ratio = 2000). Thus the Au-content of the mineralizing fluids was probably between 10 and 100 ppb.

Pyrite ($\pm$pyrrhotite) is an ubiquitous mineral in many base metal sulfide deposits; in the pyrite stability field, fluids with 10–100 ppb of gold are mostly undersaturated with respect to gold at 350°C and generally supersaturated at 250°C (Fig. 15). Under these conditions, low temperatures are necessary for gold to precipitate in equilibrium with pyrite. At 350°C, if no other mechanisms of gold precipitation occur, gold will precipitate as a primary mineral only at low values of log aH$_2$S and in a reduced environment in equilibrium with pyrrhotite and/or magnetite. Otherwise gold will be incorporated as invisible gold in pyrite or arsenopyrite. Thus here again cooling may be an effective method for gold precipitation.

Substantial amounts of gold may be transported in chemical conditions where bisulfide complexes predominate (AuHS° or Au(HS)$_2^-$) against chloride gold-bearing species (AuCl$_2^-$). Thus, Au solubility will be very sensitive to a decrease in the total activity of reduced sulfur species. In natural environments, such a reduction may be caused by various geological processes: direct precipitation of sulfur or sulfate minerals, dilution and mixing with an H$_2$S-poor brine (seawater), boiling processes, sulfidization of wall rocks, or a change in fO$_2$. Figure 16 illustrates the effect various pH-redox paths on the solubility of gold computed as a function of log fO$_2$ and pH at 350°C, with $\Sigma Na = \Sigma Cl = 0.5$. In this calculation, the total sulfur content (ΣS) is variable and the pH depends on the sulfide ($\pm$sulfate) content of the solution; high and low ΣS correspond to low and high pH respectively. This diagram also shows equal activity boundaries for sulfate and sulfide.

H$_2$S dominates in most of the pH-fO$_2$ conditions investigated. The chlorine gold-bearing species is dominant for very low sulfur contents. Therefore, gold is highly soluble (>10 ppb) as AuCl$_2^-$, in equilibrium only with hematite and can be precipitated with increasing pH, sulfate precipitation (gypsum, anhydrite) or with increasing fO$_2$. Gold is also highly soluble (100 ppb −10 ppm) in the pyrite field as Au(HS)$_2^-$, indicating that it may be transported in equilibrium with pyrite while AuHS° controls gold solubility for intermediate ΣS (0.001–0.01 m) and pH close to neutrality. If gold is transported as bisulfide, a decrease in aH$_2$S caused by the precipitation of sulfide minerals (FeS$_2$, FeS, FeAsS, PbS, ZnS, CuFeS$_2$), sulfidization of wall-rocks or mixing with H$_2$S-poor water, may cause the precipitation of gold. In this system, oxidation can be an effective mechanism for gold precipitation, but only in high fO$_2$ environments near the Py-Hm boundary. Reduction appears not to play an essential role for gold deposits in the Py, Po, or Mt stability fields.

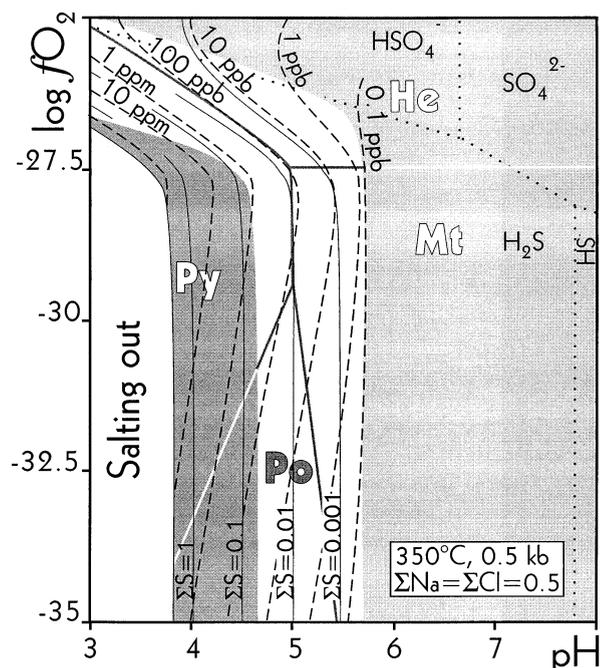These calculations demonstrate the complexity of gold-de-

Fig. 16. Solubility contours for gold in a solution of T=350°C, $\Sigma Na = \Sigma Cl = 0.5$ m, shown as a function of fO$_2$ and pH. The dashed lines represent the solubility contours of gold ($\Sigma Au = m$AuCl$_2^-$ + mAuHS° + mAu(HS)$_2^-$). The heavy lines separate the stability fields of pyrite, pyrrhotite, magnetite, and hematite. The thin solid lines represent isovalues of ΣS. The shaded areas represent the predominance fields of Au(HS)$_2^-$ and AuCl$_2^-$ gold-bearing species for low and high pH, respectively. Determination of the limit of salting-out effect in the H$_2$O-NaCl-H$_2$S system based on the data of Suleimenov and Krupp (1994) at Psat, extrapolated at 500 bars assuming identical the variation of the volatility ratio of H$_2$S and CO$_2$.

posing reactions in natural systems. Cooling, pH change, dilution, and sulfur/sulfate precipitation are some of the mechanisms which can play a role in the formation of gold deposits. In natural environments it is unlikely that the change of only one parameter would cause the precipitation of gold. For accurate chemical modelling of any ore deposit, it is essential to constrain all on these parameters. As a result, the specific natural buffers must be identified in each environment.

5. CONCLUSIONS

(1) Experiments of hydrogen diffusion show that under our experimental conditions the Ti cell can be considered a container closed to hydrogen.

(2) Stoichiometry of the dominant neutral gold-bearing species in our experiments is AuHS°. Under experimental conditions, of T = 350–450°C and P = 500 bars, AuHS° is the dominant gold-bearing species in an H$_2$O-KCl (0.5 m) solution in chemical equilibrium with the oxygen-sulphur buffers Py-Po-Mt or Py-Mt-Hm and the pH buffer quartz-K-feldspar-muscovite.

(3) The log equilibrium constants for the reaction at $Au_{(s)}$ + $H_2S_{(aq)}$ = $AuHS°$ + $\frac{1}{2} H_{2(g)}$ at 350°C, 400°C, and 450°C were determined as -5.20 ± 0.25, -5.30 ± 0.15, and -5.40 ± 0.15 respectively. These values are in good

agreement with those of Hayashi and Ohmoto (1991) and Zotov (written pers. commun.) and seems consistent with the Shenberger and Barnes (1989) study, but are significantly higher than those given by Benning and Seward (1996).

(4) In a temperature range of 250–400°C, $AuHS°$ becomes the dominant gold-bearing species in most ore-forming conditions. The $AuHS_2^-$ species becomes important at a pH above 5.5. The $AuCl_2^-$ species is important only in H_2S poor brines at 350°C. At temperatures above 400°C, $AuCl_2^-$ becomes important for gold transport in acidic solutions in equilibrium with Py-Po-Mt and quartz-albite-paragonite buffers.

(5) Cooling, pH change, H_2S loss and oxidation appear to be effective mechanisms for gold precipitation, depending on the ore-forming conditions. Consequently, prior to the modelling of Au transport and deposition, the specific natural buffers must be identified in each deposit.

REFERENCES

Barbero J. A., McCurdy K. G., and Tremaine P. R. (1982) Apparent molal heat capacities and volumes of aqueous hydrogen sulfide and sodium hydrogen sulfide near 25°C: The temperature dependence of H_2S ionization. *Canadian J. Chem.* **60,** 1872–1880.

Barker W. W. and Parks T. C. (1986) The thermodynamic properties of pyrrhotite and pyrite: a reevaluation. *Geochim. Cosmochim. Acta* **50,** 2185–2194.

Barnes H. L. (1979) Solubilities of ore minerals. In *Geochemistry of Hydrothermal Ore Deposits* (ed. H. L. Barnes), 404–460. Wiley.

Barton P. B., Jr. and Skinner B. J. (1979) Sulfide mineral stabilities. In *Geochemistry of Hydrothermal Ore deposits,* 2nd edit. (ed. H. L. Barnes), pp. 278–403. Wiley.

Belevantsev V. I, Pescchevskii and Shamovskaya G. I. (1981) Gold(I) complexes in aqueous solution. *Isvest. sib. Otd. Acad. Nauk SSSR, Ser. Khim.* **1,** 81–87.

Benning L. G. and Seward T. M. (1993) The stability of the monohydrosulphidogold (I) complex, $AuHS°$, at temperatures between 150°C and 500°C: Preliminary results. Proc. 4th. Intl. Symp. Hydrothermal Reactions, 65–68 (abstr.).

Benning L. G. and Seward T. M. (1995) $AuHS°^-$ An important gold-transporting complex in high temperature hydrosulphide solutions (abstr.). In *Water-Rock interaction-8* (ed. Y. K. Kharaka and O. V. Chudaev), pp. 783–786. Balkema Press.

Benning L. G. and Seward T. M. (1996) Hydrosulphide complexing of Au(I) in hydrothermal solutions from 150–400°C and 500–1500 bar. *Geochim. Cosmochim. Acta* **60,** 1849–1871.

Clarke E. C. W. and Glew D. N. (1966) Evaluation of thermodynamic functions for equilibrium constants. *Trans. Faraday Soc.* **62,** 539–547.

Ellis A. J. and Giggenbach W. (1971) Hydrogen sulphide ionisation and sulphur hydrolysis in high temperature solution. *Geochim. Cosmochim. Acta* **35,** 247–260.

Gibert F., Pascal M-L, and Pichavant M. (1993) Solubility of gold in KCl (0.5m) solution under hydrothermal conditions (350–450°C, 500 bars). Proc. 4th. Intl. Symp. Hydrothermal Reactions, 65–68 (abstr.).

Gibert F. and Pascal M-L. (1992) Modélisation de la solubilité et de la spéciation de l'or en milieu hydrothermal (T = 350°C, Psat) (abstr.). *14ème R.S.T., Toulouse, Soc. Géol. Fr.* édit. Paris.

Gunter M. D., Myers J., and Girsperberg S. (1987) Hydrogen: Metal membrane. *In Hydrothermal Experimental Techniques* (ed. H. L. Barnes and G. C Ulmer), pp.100–120. Wiley.

Hannington M. D. and Scoot S. D. (1989) Gold mineralization in volcanic massive sulfides: Implication of data from active hydrothermal vents on the modern sea floor. In *the Geology of Gold Deposits: The perspective in 1988* (ed. R. R. Keays et al.); *Econ. Geol. Monogr.* **6,** 491–507.

Hayashi K. and Ohmoto H. (1991) Solubility of gold in NaCl and H_2S-bearing aqueous solutions at 250–350°C. *Geochim. Cosmochim. Acta* **55,** 2111–2126.

Helgeson H. C., Kirkhan D. H., and Flowers G. C. (1981) Theoretical prediction of the thermodynamic behavior of the aqueous electrolytes at high pressures and temperatures: IV Calculation of the activity coefficients, osmotic coefficients and apparent molal and standard and relative partial molal properties to 600°C and 5 kb. *Amer. J. Sci.* **281,** 1249–1516.

Henley R. W (1973) Solubility of gold in hydrothermal chlorine solution. *Chem. Geol.* **11,** 73–87.

Hewitt D.A. (1978) A redetermination of the faylite-magnetite-quartz equilibrium between 650 and 850°C. *Amer. J. Sci.* **278,** 715–724.

Johnson J. W. , Oelkers E. H., and Helgeson H. C. (1992) SUPCRT92: A software package for calculating the standard molal thermodynamic properties of minerals, gases, aqueous species, and reactions from 1 to 5000 bar and 0°C to 1000°C. *Computer Geosci.* **18,** 899–947.

Kesler S. E. (1973) Copper, molybdenum and gold abundance in porphyry copper deposits. *Econ. Geol.* **68,** 106–112.

Kishima N. (1989) A thermodynamic study on the pyrite-pyrrhotite-magnetite system at 300–500°C with relevance to the fugacity/concentration quotient of aqueous H_2S. *Geochim. Cosmochim. Acta* **53,** 2143–2155.

Lewkowicz I. (1996) Titanium-Hydrogen. In *Hydrogen Metal Systems* (ed. F. A. Lewis and A. Aladjem); *Solid State Phenomena* **49-50,** 239–279. Scitec Publ.

Lindsay W. T., Jr (1980) Estimation of concentration quotients for ionic equilibria in high temperature water: The model substance approach. *Proc. Intl. Water Conf.* **41,** 284–294.

Murray R. C., Jr. and Cubiciotti D. (1983) Thermodynamics of aqueous sulfur species to 300°C and potential-pH diagrams. *J. Electrochem. Soc.* **130,** 866–869.

Nikolaeva N. M., Yerenburg A., and Antinina V. A. (1972) Temperature dependence of the standard potential of halite complexes of gold. *Izvest. Sib. Otd. Akad. SSSR, Ser. Khim.* **4,** 126–129.

Pan P. and Wood S. A. (1994) Solubility of Pt and Pd sulfides and Au metal in aqueous bisulfide solutions. II. Results at 200° to 250°C and saturated vapor pressure. *Mineral. Deposita* **29,** 373–390.

Pokroskii V. A. and Helgeson H. C. (1995) Thermodynamic properties of aqueous species and the solubilities of minerals at high pressures and temperatures: The system Al_2O_3-H_2O-NaCl. *Amer. J. Sci.* **295,** 1255–1342.

Renders P. J. and Seward T. M. (1989) The stability of hydrosulphido- and sulfido-complexes of Au(I) and Ag(I) at 25°C. *Geochim. Cosmochim. Acta* **53,** 245–253.

Rytuba J. J. and Dickson F. W. (1977) Reaction of pyrite + pyrrhotite + quartz + gold with NaCl-H_2O solutions, 300–500°C, 500 to 1500 bars and genetic implications. *4th IAGOD Symp.* Varnia, Bulgarian Acad. Sciences Sofia, II, 1974.

Scott S. D. and Barnes H. L. (1972) Sphalerite geothermometry and geobarometry. *Econ. Geol.* **66,** 653–669.

Seward T. M. (1973) Thio complexes of gold and the transport of gold in hydrothermal ore solutions. *Geochim. Cosmochim. Acta* **37,** 370–399.

Seward T. M. (1984) The transport and deposition of gold in hydrothermal system. In *Gold '82: The Geology, Geochemistry, and Genesis of Gold Deposits* (ed R. P. Foster), pp. 165–181. A. A. Blakeman.

Seyfried W. E., Janeky D. R., and Berndt M. E. (1987) Rocking autoclaves for hydrothermal experiments II: The flexible reaction-cell system. In *Hydrothermal experimental techniques* (ed. G. C Ulmer and H. L. Barnes), pp. 216–239. Wiley.

Shaw H.R. (1963) Hydrogen-water mixtures; control of hydrothermal experiments by hydrogen osmosis. *Science* **139,** 1220–1222.

Shenberger D. M. and Barnes H. L. (1989) Solubility of gold in aqueous sulfides solutions from 150 to 350°C. *Geochim. Cosmochim. Acta* **53,** 269–278.

Shock E. L., Helgeson H. C., and Sverjensky D. A. (1989) Calculation of the thermodynamic and transport properties of aqueous species at high pressures and temperatures: Standard partial molal properties of inorganic neutral species. *Geochim. Cosmochim. Acta* **53,** 2157–2183.

Shock E. L., Oelkers E. H., Johnson J. W, Sverjensky D. A., and Helgeson H. C. (1992) Calculation of the thermodynamic and transport properties of aqueous species at high pressures and temperatures: Effective electrostatic radii, dissociation constants, and standard partial molal properties to 1000°C and 5 kbar. *J. Chem. Soc. London, Faraday Trans.* **88,** 803–826.

Shock E. L., Sassani D.C., Willis M., and Sverjensky D. A. (1997) Inorganic species in geologic fluids: Correlations among standard molal thermodynamic properties of aqueous ions and hydroxide complexes. *Geochim. Cosmochim. Acta* **61,** 907–950.

Sretenskaya N. G. (1977) Dissociation of hydrogen sulfide under pressure. *Geochem. Intl.* **3,** 430–438.

Suleimenov O. M. and Krupp R. E. (1994) Solubility of hydrogen sulphide in pure water and in NaCl solutions, from 20 to 320°C and at saturation pressures. *Geochim. Cosmochim. Acta* **58,** 2433–2444.

Suleimenov O. M. and Seward T. M. (1997) A Spectrophotometric study of hydrogen sulphide ionisation in aqueous solutions to 350°C. *Geochim. Cosmochim. Acta* **61,** 5187–5198.

Sverjensky D. A., Hemley J. J., and d'Angelo W. M. (1991) Thermo-dynamic assessment of hydrothermal alkali feldspar-mica-alumino-silicate equilibria. *Geochim. Cosmochim. Acta* **55,** 989–1004.

Sverjensky D. A., Shock E. L., and Helgeson H. C. (1997) Prediction of the thermodynamic properties of aqueous metal complexes to 1000°C and 5 kb. *Geochim. Cosmochim. Acta* **61,** 1359–1412.

Tagirov B.R, Zotov A.V., and Akinfiev N.N. (1997) Experimental study of dissociation constants of HCL from 350 to 500°C and from 500 to 2500 bars: Thermodynamic properties of HCl°(aq). *Geochim. Cosmochim. Acta* 61, 4267–4280.

Toulmin P. III and Barton P. B., Jr. (1964) A thermodynamic study of pyrite and pyrrhotite. *Geochim. Cosmochim. Acta* **28,** 641–671.

Tsonopoulos C., Coulson D. M. , and Inman L. B. (1976) Ionization constants of water polluants. *J. Chem. Eng. Data* **21,** 190–193.

Wood S. A., Crerar D. A., and Borscik M.P. (1987) Solubility of the assemblage pyrite-pyrrhotite-magnetite-sphalerite-galena-gold-stib-ine-bismuthinite-argentite-molybdenite in H_2O-NaCl-CO_2 solution from 200 to 350°C. *Econ. Geol.* **82,** 1864–1887.

Wood S. A., Pan P., Zhang Y., and Mucci A. (1994) Solubility of Pt and Pd sulfides and Au metal in aqeous bisulfide solutions I. Results at 25°–90°C and 1 atm. *Mineral. Deposita* **29,** 309–317.

Zotov A. V. and Baranova N. N. (1989) Thermodynamic properties of aurochloride solute complex $AuCl_2^-$ at temperature of 350–500°C and pressure of 500–1500 bars. *Sci. Géol. Bull.* **42,** 355–342.

Zotov A. V. and Baranova N. N. (1995) The solubility of Au_2S and AuAgS in near-neutral sulphide solutions at temperatures of 25 and 80°C and pressures of 1 and 500 bars. In *Water-Rock Inter-action-8* (ed Y. K. Kharaka and O. V. Chudaev), pp. 113–115. Balkema Press.

Table A1. Selected equilibrium constants used in this study

		P$_{sat}$					500 bar							
	25°C	150°C	200°C	250°C	300°C	350°C	150°C	200°C	250°C	300°C	350°C	400°C	450°C	
(R1) $H_2(g) + \frac{1}{2} O_2(g) = H_2O$		26.85	23.18	20.22	17.80	15.78	26.73	23.07	20.13	17.71	15.70	14.01	12.57	1
(R2) $H_2S(aq) + \frac{1}{2} O_2(g) = H_2O + \frac{1}{2} S_2(g)$		20.02	17.49	15.41	13.65	12.12	20.13	17.58	15.48	13.72	12.21	10.87	9.59	1
(R3) $FeS_2 = FeS + \frac{1}{2} S_2(g)$		−10.32	−8.50	−7.01	−5.78	−4.73	−10.29	−8.47	−6.99	−5.76	−4.72	−3.83	−3.06	1
(R4) $Fe_3O_4 + 3 S_2(g) = 3 FeS_2 + 2 O_2(g)$		−40.63	−37.79	−35.51	−33.64	−32.09	−40.80	−37.94	−35.64	−33.75	−32.17	−30.84	−29.70	1
(R5) $2 FeS + Fe_3O_4 + 8 H^+ = 4 Fe^{2+} + FeF_2 + 4 H_2O$		26.34	21.36	17.11	13.29	10.12	26.88	21.95	17.83	14.28	11.06	9.97	11.95	1
(R6) $2 Fe_3O_4 + \frac{1}{2} O_2(g) = 3 Fe_2O_3$		23.45	20.24	17.65	15.51	13.70	23.44	20.23	17.64	15.50	13.69	12.15	10.81	1
(R7) $3 KAlSi_3O_8 + 2 H^+ = 2K^+ + 6 SiO_2 + KAl_3Si_3O_{10}(OH)_2$		8.31	7.99	7.70	7.42	7.14	8.48	8.14	7.85	7.58	7.32	7.13	6.93	1
(R8) $Au(HS)_2^- + \frac{1}{2} H_2(g) = H_2(g) + HS + Au(s)$		2.64	2.14	1.77	1.50	1.34	2.84	2.25	1.85	1.50	1.30	1.25	1.20	2
(R9) $HAu(HS)_2^- + \frac{1}{2} H_2(g) = 2 H_2S(aq) + Au(s)$						4.00								3
(R10) $AuHS° + \frac{1}{2} H_2(g) = H_2S(aq) + Au(s)$		5.90	5.40	5.20	5.10	5.00	6.15	5.65	5.45	5.35	5.20	5.25	5.30	4
(R11) $AuCl_2^- + \frac{1}{2} H_2(g) = 2Cl^- + H^+ + Au(s)$		11.26	8.97	6.90	4.90	2.70	11.35	9.10	7.11	5.28	3.48	1.82	−0.46	5
(R12) $FeCl^+ = Cl^- + Fe^{2+}$		−0.61	−1.09	−1.69	−2.45	−3.52	−0.52	−0.96	−1.47	−2.05	−2.79	−3.36	−4.30	1
(R13) $FeCl_2^° = 2 Cl^- + Fe^{2+}$		1.05	0.17	−0.92	−2.34	−4.43	1.24	0.45	−0.48	−1.56	−2.92	−4.02	−5.96	1
(R14) $Fe^{2+} + H_2O = Fe(OH)^+ + H^+$		−6.63	−5.94	−5.35	−4.84	−4.47	−6.45	−5.79	−5.24	−4.77	−4.35	−4.31	−4.58	6
(R15) $Fe^{2+} + 2 H_2O = Fe(OH)_2^° + 2 H^+$		−14.60	−13.11	−11.88	−10.80	−9.97	−14.41	−12.99	−11.83	−10.84	−9.97	−9.73	−10.13	6
(R16) $HCl° = H^+ + Cl^-$		0.53	0.10	−0.47	−1.22	−2.33	0.70	0.29	−0.23	−0.86	−1.63	−2.51	−4.12	7
(R17) $KOH° = K^+ + OH^-$		−0.10	−0.26	−0.50	−0.91	−1.72	−0.81	−0.92	−1.08	−1.31	−1.69	−2.04	−2.87	8
(R18) $KCl° = K^+ + Cl^-$		0.58	0.22	−0.20	−0.74	−1.64	0.68	0.35	0.00	−0.39	−0.91	−1.49	−2.87	1
(R19) $KHS° = K^+ + HS^-$		0.58	0.22	−0.20	−0.74	−1.64	0.68	0.35	0.00	−0.39	−0.91	−1.49	−2.87	9
(R20) $H_2S(aq) = HS^- + H^+$		−6.50	−6.68	−7.02	−7.56	−8.50	−6.37	−6.53	−6.82	−7.21	−7.78	−8.49	−10.06	1
(R21) $H_2O = H^+ + OH^-$		−11.63	−11.28	−11.17	−11.30	−11.83	−11.46	−11.09	−10.81	−10.90	−11.11	−11.36	−12.19	1
(R22) $H_2(g) = H_2(aq)$	−3.105	−2.98	−2.81	−2.61	−2.38	−2.07	−3.15	−2.97	−2.76	−2.54	−2.28	−1.96	−1.39	1
(R23) $NaOH° = Na^+ + OH^-$		0.34	−0.06	−0.61	−1.42	−2.87	0.41	0.07	−0.36	−0.91	−1.70	−2.64	−4.92	10
(R24) $NaCl° = Na^+ + Cl^-$		0.21	−0.09	−0.48	−1.01	−1.92	0.30	0.03	−0.29	−0.67	−1.18	−1.74	−3.05	1
(R25) $NaHS° = Na^+ + HS^-$		0.21	−0.09	−0.48	−1.01	−1.92	0.30	0.03	−0.29	−0.67	−1.18	−1.74	−3.05	11
(R26) $SO_4^{2-} + 2 H^+ = H_2S(aq) + 2 O_2(g)$		−79.21	−66.97	−56.71	−47.75	−39.29	−79.40	−67.22	−57.08	−48.39	−40.66	−33.77	−26.18	1
(R27) $HSO_4^- = H^+ + SO_4^{2-}$		−3.72	−4.47	−5.26	−6.18	−7.40	−3.56	−4.28	−5.01	−5.78	−6.65	−7.44	−8.76	1
(R28) $FeS_2 + 2 H^+ + H_2(g) = Fe^{2+} + 2 H_2S(aq)$		−1.61	−1.26	−0.94	−0.66	−0.27	−1.75	−1.35	−0.97	−0.60	−0.27	0.55	2.27	1
(R29) $FeS + 2H^+ = Fe^{2+} + H_2S(aq)$		1.88	1.55	1.25	0.97	0.80	1.93	1.62	1.38	1.16	0.96	1.25	2.36	1
(R30) $Fe_3O_4 + H_2(g) + 6 H^+ = 3 Fe^{2+} + 4 H_2O$		20.96	17.00	13.67	10.70	8.25	21.26	17.35	14.12	11.36	8.88	8.03	9.52	1
(R31) $Fe_2O_3 + H_2(g) + 4 H^+ = 2 Fe^{2+} + 3 H_2O$		15.11	12.31	9.97	7.90	6.19	15.27	12.51	10.24	8.31	6.59	5.96	6.93	1
Qtz-FK-Musc $\quad K^+/H^+$		4.16	3.99	3.85	3.71	3.57	4.24	4.07	3.92	3.79	3.66	3.56	3.46	1
Py-Po-Mt $\quad Fe^{2+}/(H^+)^2$		6.43	5.24	4.13	3.17	2.38	6.57	5.34	4.31	3.42	2.61	2.34	2.84	1
Qtz-Ab-Par $\quad Na^+/H^+$									4.76	4.48	4.23	4.08	3.98	1

Sources: 1. SUPCRT92, Johnson et al. (1992); 2. This study recalculated from Shenberger and Barnes (1989) at Psat, extrapolated at 500 bar; 3. Hayashi and Ohmoto (1991); 4. This study extrapolated from measured gold solubility at 350-450°C and 500 bar; 5. Zotov and Baranova (1989); 6. Shock et al. 1997; 7. Tagirov et al. (1997); 8. Sverjensky et al. (1991); 9. Assumed identical to the dissociaiton constant of KOH; 10. Pokrovskii and Helgeson (1995); 11. Assumed identical to the dissociation constant of NaOH.